mathematics

Article

Investigation of Size-Dependent Vibration Behavior of Piezoelectric Composite Nanobeams Embedded in an Elastic Foundation Considering Flexoelectricity Effects

Alaa A. Abdelrahman [1], Mohamed S. Abdelwahed [2], Hani M. Ahmed [3], Amin Hamdi [3] and Mohamed A. Eltaher [2,*]

[1] Mechanical Design & Production Department, Faculty of Engineering, Zagazig University, P.O. Box 44519, Zagazig 44519, Egypt

[2] Mechanical Engineering Department, Faculty of Engineering, King Abdulaziz University, P.O. Box 80204, Jeddah 21589, Saudi Arabia

[3] Department of Civil and Environmental Engineering, Faculty of Engineering, King Abdulaziz University, P.O. Box 80204, Jeddah 21589, Saudi Arabia

* Correspondence: meltaher@kau.edu.sa or mohaeltaher@gmail.com; Tel.: +966-565518613 or +20-1001089561

Abstract: This article investigates the size dependent on piezoelectrically layered perforated nanobeams embedded in an elastic foundation considering the material Poisson's ratio and the flexoelectricity effects. The composite beam is composed of a regularly squared cut-out elastic core with two piezoelectric face sheet layers. An analytical geometrical model is adopted to obtain the equivalent geometrical variables of the perforated core. To capture the Poisson's ratio effect, the three-dimensional continuum mechanics adopted to express the kinematics are kinetics relations in the framework of the Euler–Bernoulli beam theory (EBBT). The nonlocal strain gradient theory is utilized to incorporate the size-dependent electromechanical effects. The Hamilton principle is applied to derive the nonclassical electromechanical dynamic equation of motion with flexoelectricity impact. A closed form solution for resonant frequencies is obtained. Numerical results explored the impacts of geometrical and material characteristics on the nonclassical electromechanical behavior of nanobeams. Obtained results revealed the significant effects of the mechanical, electrical, and elastic foundation parameters on the dynamic behavior of piezoelectric composite nanobeams. The developed procedure and the obtained results are helpful for many industrial purposes and engineering applications, such as micro/nano-electromechanical systems (MEMS) and NEMS.

Keywords: piezoelectric composite nanobeam; perforated core; Pasternak elastic foundation; regularly squared cut-out; electromechanical effects; equivalent geometrical variables; nonlocal strain gradient theory; flexoelectricity

MSC: 74f15

Citation: Abdelrahman, A.A.; Abdelwahed, M.S.; Ahmed, H.M.; Hamdi, A.; Eltaher, M.A. Investigation of Size-Dependent Vibration Behavior of Piezoelectric Composite Nanobeams Embedded in an Elastic Foundation Considering Flexoelectricity Effects. *Mathematics* **2023**, *11*, 1180. https://doi.org/10.3390/math11051180

Academic Editors: Subrat Kumar Jena, Snehashish Chakraverty, Dineshkumar Harursampath, Francesco Tornabene and José R. Fernánde

Received: 13 January 2023
Revised: 21 February 2023
Accepted: 23 February 2023
Published: 27 February 2023

1. Introduction

The usage of flexoelectric nanobeams is a newer generation of nanotechnology industrial applications, such as actuators, sensors, energy harvesters, biology, medical science, etc. Flexoelectricity depicts the coupling between electric polarizations and mechanical strain gradients. The flexoelectric effects have been considered in the industry because it has different crystalline structures as piezoelectric materials [1].

For piezo/flexo-electricity analysis, Liang et al. [2] included the surface influence on a piezoelectric nanobeam and found that bulk flexoelectricity is increased and deflection is decreased by increasing the surface effects. Bhaskar et al. [3] manufactured flexoelectric cantilever nanobeam with a single flexoelectrically active layer. Baroudi et al. [4] developed analytical static and dynamic responses of piezoelectric–flexoelectric nanobeams in frame of a strain gradient theory. Chu et al. [5] presented the flexoelectric effects on mechanical responses of functionally graded (FG) piezoelectric modified strain gradient nanobeams by using the Navier analytical method. Ebrahimi and Karimiasl [6] analytically studied the buckling behavior of flexoelectric sandwich nonlocal nanobeams with surface effects. Wang et al. [7] developed a reduced order model for an array of flexoelectric layered nanobeams to provide higher electrical power output and wider frequency bandwidth. Shijie et al. [8] presented the influences of flexoelectricity, piezoelectricity, dielectricity, and surface elasticity on the buckling stability of nanobeam by using the finite element method. Basutkar [9] derived analytical solutions of bimorph piezoelectric–flexoelectric cantilever energy harvester. Eltaher et al. [10,11] developed a modified continuum model to investigate static and vibration behaviors of perforated piezoelectric nanobeam in the frame of nonlocal elasticity and surface energy. Zhao et al. [12] numerically studied the influences of porosity and flexoelectricity on static and vibration of FG piezoelectric nanobeams. Malikan and Eremeyev [13] investigated the effect of flexoelectricity on a piezoelectric nanobeam involving internal viscoelasticity.

Malikan and Eremeyev [14] evaluated the nonlinear bending of a piezo–flexomagnetic strain gradient nanobeam based on an analytical-numerical solution. Malikan [15] and Malikan and Eremeyev [16] examined the nonlinear buckling of the electro-mechanical and flexomagnetic nanoplate, including the nonlinear strains of von Karman. Bagheri and Tadi Beni [1] analyzed the flexoelectric forced response of viscoelastic Euler nanobeams incorporating von Karman strain–displacement nonlinearities. Esen et al. [17,18] analytically examined the natural frequencies and buckling loads of a cracked FG microbeam exposed to magnetic and thermal environments. Wang et al. [19] exploited nonlocal Donnell's nonlinear shell theory in analyzing the vibration of FG piezoelectric nanoshells. Liu et al. [20,21] solved vibrations of FG piezoelectric shells in a multi-physics field and rested on an elastic foundation. Gao et al. [22] investigated wave propagation of FG metal foam plates with piezoelectric actuator and sensor layers. Melaibari et al. [23] developed a mathematical model to examine vibration response of a sandwich perforated nanobeam incorporating the flexoelectricity effect. Jena et al. [24] developed a novel numerical approach to study the stability of a nanobeam embedded in an elastic foundation and exposed to hygro–thermo–magnetic environments. Sun et al. [25] developed a finite element model to predict the flexoelectric nonlocal nanobeam energy harvesters with a nonuniform cross-section. Thai et al. [26] proved the effects of geometry, topology, and materials on the nonlinear vibration response of curved flexoelectric–piezoelectric microbeam energy harvesting. Momeni-Khabisi and Tahani [27] developed a solution procedure to investigate the stability of piezomagnetic nanosensors, including flexomagnetic, thermal, and geometrical imperfection effects.

In the frame of nonlocal strain gradient theory, Jena et al. [28] studied the vibrational response of micro/nanoobeam rested on various types of Winkler elastic foundations. Jena et al. [29,30] examined the vibration of the nonlocal strain gradient single-walled carbon nanotube under the hygro–magnetic environment and nonlinear temperature distribution. Malikan et al. [31] examined the torsional stability capacity of a nano-composite first-order shear deformation shell under a three-dimensional magnetic field. Karami et al. [32] investigated the vibration response of a 2D-tapered porous FG Timoshenko beam, including temperature and porosity influences on the material properties. Chakraverty and Jena [33] studied the vibration of single-walled carbon nanotubes (SWCNT) and single-layered graphene nanoribbons resting on exponentially varying Winkler elastic foundations using the differential quadrature method. Abdelrahman et al. [34] studied the effects of a moving load on the vibration response of reinforced FG nanobeams rested on a foundation. Tocci Monaco et al. [35] examined the magneto–electro–elastic static response of nanoplates in a hygro–thermal environment. Ghandourah et al. [36] examined static and buckling behaviors of FG-laminated nanoplates by quasi-3D hyperbolic shear theory. Alazwari et al. [37] derived a model to investigate the dynamic response of FG nanobeams under thermo–magnetic fields and a moving load. Alam and Mishra [38] studied the post stability of nonlocal strain gradient FG piezoelectric cylindrical shells under thermo–electro–mechanical loads. Boyina and Piska [39] studied the impact of surface and magnetic field effects on the wave propagation response of viscoelastic nanobeams.

According to the shortlisted literature and the authors' backgrounds, influences of the material Poisson's ratio and the elastic foundation on the nonclassical electromechanical dynamic behavior of piezoelectric composite nanobeams with the flexoelectricity effect has not been considered. This present work develops an analytical nonclassical procedure to investigate the size-dependent electromechanical free vibration behavior of piezoelectric composite nanobeam with a perforated core resting on an elastic foundation with the flexoelectricity effect based on the nonlocal strain gradient theory. In the context of continuum mechanics, all kinematics and kinetics equations are developed based on the Euler–Bernoulli beam theory. Regular squared cut-outs perforation configuration is considered for the elastic perforated core. Hamilton's principle is adopted to obtain the nonclassical electromechanical dynamic equation of motion, including the elastic foundation as well as the flexoelectricity effects. The accuracy of the proposed procedure is checked, and good agreement is obtained. Numerical results are obtained and discussed. Conclusions and recommendations are summarized.

2. Theory and Mathematical Formulation

Consider a composite piezoelectric nanobeam with a regularly squared perforated core and two piezoelectric face sheets embedded in two elastic foundation parameters, as shown in Figure 1. The top and bottom face layers are assumed to be made of the same material, and each has height h_p. The perforated core is assumed to be made of an elastic material with elasticity modulus E_c, and it has a height of h_c. All layers have the same beam length L and width W_b. The entire composite beam thickness is h, and $h = h_c + 2h_p$. The polarization direction of both piezoelectric face sheets is assumed upward. Mathematical formulations of the physical phenomena will be presented in the following subsections.

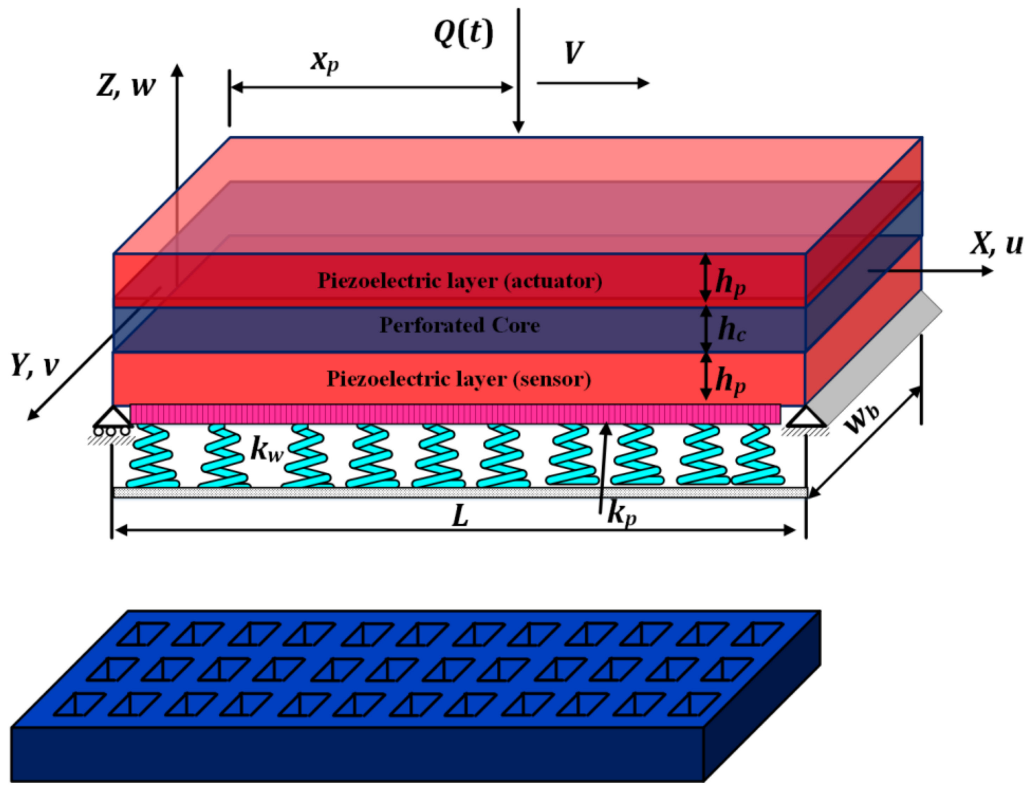

Figure 1. Perforated composite piezoelectric nanobeam rested on elastic foundation.

2.1. Geometrical Model for Regular Squared Cutouts

Consider a regularly squared perforation pattern, as shown in Figure 1, with the following geometrical variables: l_s and $l_s - t_s$, are a spatial period, a hole side, respectively. *N is* the number of hole rows through a beam width. The filling ratio, α can be given by [40,41]:

$$\alpha = \frac{t_s}{l_s} \qquad 0 \leq \alpha \leq 1, \qquad \alpha = \begin{cases} 0 & \text{Fully perforated (artifitial case)} \\ 1 & \text{Fully filled (solid beam)} \end{cases} \tag{1}$$

The bending (EI) and shear (GA) stiffness ratios for perforated and full beam are

$$\overline{K}_b = \frac{(EI)_{eq}}{(EI)_s} = \left\{ \frac{\alpha(N+1)\left(N^2+2N+\alpha^2\right)}{(1-\alpha^2+\alpha^3)N^3+3\alpha N^2+(3+2\alpha-3\alpha^2+\alpha^3)\alpha^2 N+\alpha^3} \right\} \tag{2}$$

$$\overline{K}_s = \frac{(GA)_{eq}}{(EA)_s} = \left(\frac{(1+N)\alpha^3}{2N} \right) \tag{3}$$

where subscripts $(:)_{eq}$, $(:)_s$ are equivalent and fully filled solid beams, respectively. The equivalent mass and inertia ratios are [41]

$$\overline{I}_A = \frac{(\rho A)_{eq}}{(\rho A)_s} = \left\{ \frac{[1-N(\alpha-2)]\alpha}{N+\alpha} \right\} \tag{4}$$

$$\overline{I}_B = \frac{(\rho I)_{eq}}{(\rho I)_s} = \left\{ \frac{\alpha\left[(2-\alpha)N^3+3N^2-2(\alpha-3)\left(\alpha^2-\alpha+1\right)N+\alpha^2+1\right]}{(N+\alpha)^3} \right\} \tag{5}$$

2.2. Basic Elastic and Flexoelectric Kinematic Relations

The displacement and the electric fields for Euler–Bernoulli beam theory (EBBT) can be prescribed by [38]:

$$\begin{Bmatrix} u(x,z,t) \\ w(x,z,t) \\ E_z \end{Bmatrix} = \begin{Bmatrix} -z\frac{\partial w(x,t)}{\partial x} \\ w(x,t) \\ -\frac{\partial \phi_z(z,t)}{\partial z} \end{Bmatrix} \tag{6}$$

where $w(x,t)$ and $\phi_z(z,t)$ refer to the transverse displacement and the electric potential field, respectively.

Based on the described displacement field, the nonzero strain component is given by [42,43]:

$$\varepsilon_{xx}(x,z,t) = -z\frac{\partial^2 w(x,t)}{\partial x^2} \tag{7}$$

Considering an isotropic elastic material behavior for the perforated core, the material constitutive law for the EBBT could be expressed as [44]:

$$\begin{Bmatrix} \sigma_{xx}(x,z,t) \\ \sigma_{yy(x,z,t)} \\ \sigma_{zz}(x,z,t) \end{Bmatrix} = \begin{Bmatrix} \hat{E}\varepsilon_{xx}(x,z,t) \\ \lambda\varepsilon_{xx}(x,z,t) \\ \lambda\varepsilon_{xx}(x,z,t) \end{Bmatrix} = \begin{Bmatrix} \frac{(1-\nu)E}{(1+\nu)(1-2\nu)}\left(-z\frac{\partial^2 w(x,t)}{\partial x^2}\right) \\ \lambda\left(-z\frac{\partial^2 w(x,t)}{\partial x^2}\right) \\ \left(\frac{\nu}{1-\nu}\right)\sigma_{xx}(x,z,t) \end{Bmatrix} \tag{8}$$

where $\hat{E} = 2\mu + \lambda$ refers to the equivalent elasticity modulus, v is the Poisson's ratio, σ_{xx}, σ_{yy}, and σ_{zz} are the components of the Cauchy normal stress tensor, respectively. λ and μ are Lame's constants that can be expressed by:

$$\mu = \frac{E}{2(1+\nu)}, \qquad \lambda = \frac{\nu E}{(1+\nu)(1-2\nu)} \tag{9}$$

Taking into accounts the electric and flexoelectric effects, the electric enthalpy energy density function is expressed as [2]:

$$H = -\frac{1}{2}a_{kl}E_kE_l + \frac{1}{2}c_{ijkl}\varepsilon_{ij}\varepsilon_{kl} - e_{ijk}\ E_k\ \varepsilon_{ij} - u_{ijkl}\ E_i\ \varepsilon_{jk,l} \tag{10}$$

where a_{kl} refers to permittivity tensor, c_{ijkl} denotes elasticity tensor, e_{ijk} refers to piezoelectric coefficients, u_{ijkl} is the electric field strain gradient coupling coefficients.

The electric field is presented in terms of the electric enthalpy energy by:

$$D_i = -\frac{\partial H}{\partial E_i} = a_{ij}E_j + e_{ijk}\ \varepsilon_{jk} + u_{ijkl}\ \varepsilon_{jk,l} \tag{11}$$

Based on the Gaussian theorem, the following condition is verified:

$$\frac{\partial D_z}{\partial z} = 0 \Rightarrow a_{33}\frac{\partial E_z}{\partial z} + e_{311}\ \frac{\partial \varepsilon_{xx}}{\partial z} + u_{3111}\frac{\partial^2 \varepsilon_{xx}}{\partial x \partial z} + u_{3113}\frac{\partial^2 \varepsilon_{xx}}{\partial z^2} = 0. \tag{12}$$

Substituting Equation (8) into Equation (12), yields

$$a_{33}\frac{\partial E_z}{\partial z} - e_{311}\ \left(\frac{\partial^2 w(x,t)}{\partial x^2}\right) - u_{3111}\left(\frac{\partial^3 w(x,t)}{\partial x^3}\right) = 0. \tag{13}$$

Rearranging terms in Equation (13), the 1st derivative of the electric field is given by:

$$\frac{\partial E_z}{\partial z} = \frac{1}{a_{33}}\left[e_{311}\ \left(\frac{\partial^2 w(x,t)}{\partial x^2}\right) + u_{3111}\left(\frac{\partial^3 w(x,t)}{\partial x^3}\right)\right] \tag{14}$$

Integrating Equation (14) with respect to z one can write:

$$E_z - E_{z0} = \frac{z}{a_{33}}\left[e_{311}\ \left(\frac{\partial^2 w(x,t)}{\partial x^2}\right) + u_{3111}\left(\frac{\partial^3 w(x,t)}{\partial x^3}\right)\right] \tag{15}$$

Equation (15) can be rewritten as:

$$E_z = E_{z0} - \frac{1}{a_{33}}\left[e_{311}\ (\varepsilon_{xx}) + u_{3111}\left(\frac{\partial \varepsilon_{xx}}{\partial x}\right)\right], \tag{16}$$

in which E_{z0} is initial electric field through thickness direction.

2.3. *The Modified Nonlocal Strain Gradient Theory with Flexoelectricity Effect*

According to the nonlocal strain gradient theory (NSGT), the stress field, including the flexoelectricity effect and nonlocal electric potential, can be presented by [45,46]:

$$\left(1-(e_0a)^2\frac{\partial^2}{\partial x^2}\right)\begin{Bmatrix}\sigma^t_{xx}\\ \sigma_{113}\\ \sigma_{111}\\ D_z\end{Bmatrix} = \begin{Bmatrix}\left\{E\left(1-l^2\frac{\partial^2}{\partial x^2}\right)+\frac{e_{311}^2}{a_{33}}\right\}\varepsilon_{xx} + \frac{e_{311}}{a_{33}}\mu_{3111}\frac{\partial \varepsilon_{xx}}{\partial x} - e_{311}E_{z0}\\ \frac{\mu_{3113}}{a_{33}}\left(e_{311}\varepsilon_{xx}+\mu_{3111}\frac{\partial\varepsilon_{xx}}{\partial x}\right) - \mu_{3113}E_{z0}\\ \frac{\mu_{3111}}{a_{33}}\left(e_{311}\varepsilon_{xx}+\mu_{3111}\frac{\partial\varepsilon_{xx}}{\partial x}\right) - \mu_{3111}E_{z0}\\ a_{33}E_{z0}+\mu_{3113}\frac{\partial\varepsilon_{xx}}{\partial z}\end{Bmatrix} \tag{17}$$

3. Dynamic Equation of Motion of Piezoelectric Composite Nanobeam

Applying the Hamiltonian principle, the dynamic equation of motion is given as [47,48]:

$$\delta\int_{t_1}^{t_2}\left[T - \int_\Omega Hd\Omega + W_{ex}\right]dt = 0 \tag{18}$$

with Ω indicates a volume integral, T is the total kinetic energy of the composite beam. The variation in the total kinetic energy, δT can be expressed as:

$$\begin{aligned}\delta T &= \delta\left\{\tfrac{1}{2}\int_\Omega \rho\left(\dot{u}^2+\dot{w}^2\right)d\Omega\right\}\\ &= \int_0^L\left\{\left([\rho_c I_c]_{eq}+\rho_p I_p\right)\tfrac{\partial^4 w}{\partial x^2\partial t^2}-\left([\rho_c A_c]_{eq}+2\rho_p A_p\right)\tfrac{\partial^2 w}{\partial t^2}\right\}\delta w dx,\end{aligned} \tag{19}$$

With

$$\begin{bmatrix} I_c & I_p & A_c & A_p\end{bmatrix} = \begin{bmatrix}\frac{h_c^3}{12} & \frac{h^3}{12}-I_c & h_c w_b & h_p w_b\end{bmatrix} \tag{20}$$

On the other hand, the variation in the electric enthalpy energy density function, $\delta\int_\Omega H d\Omega$ can be expressed as:

$$\begin{aligned}\delta\int_\Omega H d\Omega &= \int_\Omega\left(\sigma_{xx}^t\delta\varepsilon_{xx}-D_z\delta E_z+\sigma_{111}\,\delta\varepsilon_{xx,x}+\sigma_{113}\,\delta\varepsilon_{xx,z}\right)d\Omega\\ &= \int_0^L\left(\overline{M}\delta\varepsilon_{xx0}+\overline{M}'\delta\varepsilon_{xx0,x}\right)d\mathrm{x}\end{aligned} \tag{21}$$

where

$$\begin{bmatrix}\varepsilon_{xx0} & \overline{M} & \overline{M}'\end{bmatrix} = \begin{bmatrix}-\frac{\partial^2 w}{\partial x^2} & M+\frac{e_{311}}{a_{33}}M_D+N_{113} & \frac{\mu_{3111}}{a_{33}}M_D+N_{111}\end{bmatrix} \tag{22}$$

Based on the nonlocal strain gradient elasticity theory, the following equations could be written:

$$\begin{aligned}&\left(1-(e_0 a)^2\tfrac{\partial^2}{\partial x^2}\right)\begin{Bmatrix} M\\ N_{113}\\ M_{111}\\ M_D\end{Bmatrix}\\ &= \begin{Bmatrix}\left(1-l^2\tfrac{\partial^2}{\partial x^2}\right)\left\{(E_c I_c)_{eq}-E_p I_p\right\}\varepsilon_{xx0}+\tfrac{e_{311}^2}{a_{33}}I_p\varepsilon_{xx}+\tfrac{e_{311}\mu_{3111}I_p}{a_{33}}\tfrac{\partial\varepsilon_{xx0}}{\partial x}-e_{311}I_1E_{z0}\\ 0\\ w_b\left\{\tfrac{\mu_{3111}}{a_{33}}I_p\left(e_{311}\varepsilon_{xx0}+\mu_{3111}\tfrac{\partial\varepsilon_{xx0}}{\partial x}\right)-\mu_{3111}I_1E_{z0}\right\}\\ w_b a_{33}I_1E_{z0}\end{Bmatrix}\end{aligned} \tag{23}$$

in which

$$I_1 = \frac{1}{4}\left(h^2-h_c^2\right) \tag{24}$$

The variation in the external work completed, W_{ex} is given by:

$$\delta W_{ex} = -w_b\int_0^L p(x,t)\delta w(x,t)dx \tag{25}$$

where $p(x,t) = q(x,t)D_s(x-x_p)+N_b\frac{\partial^2 w(x,t)}{\partial x^2}+\left[k_w w(x,t)-k_p\frac{\partial^2 w(x,t)}{\partial x^2}\right]$ is the applied external load function, D_s (.) is the Dirac delta function. k_w and k_p are the Winkler shear foundation constants, respectively.

Substituting Equations (19)–(25) into Equation (18), the governing equation of motion is given by:

$$\frac{\partial^2\overline{M}}{\partial x^2}-\frac{\partial^3\overline{M}'}{\partial x^3}-p(x,t) = \left[(\rho_c A_c)_{eq}+2\rho_p A_p\right]\frac{\partial^2 w}{\partial t^2}-\left[(\rho_c I_c)_{eq}+\rho_p I_p\right]\frac{\partial^4 w}{\partial x^2\partial t^2} \tag{26}$$

The governing equilibrium equations are generalized by using:

$$W = \frac{w}{h},\quad X = \frac{x}{L},\ \overline{q} = \frac{qL^3}{EI},\ \overline{P} = \frac{N_b L^2}{EI} \tag{27}$$

Then,

$$dx = LdX \quad and \quad \frac{dW}{dX} = \left(\frac{L}{h}\right)\frac{dw}{dx} \to \frac{dw}{dx} = \left(\frac{h}{L}\right)\frac{dW}{dX} \tag{28}$$

and

$$\frac{d^4w}{dx^4} = \frac{d^3}{dx^3}\left[\left(\frac{h}{L}\right)\frac{dW}{dX}\right] = \left(\frac{h}{L^4}\right)\frac{d^4W}{dX^4} \quad \text{and} \quad \frac{d^6w}{dx^6} = \left(\frac{h}{L^6}\right)\frac{d^6W}{dX^6} \tag{29}$$

Substituting from Equations (19) and (27)–(29) into Equation (26), yields the non-dimensional dynamic equation of motion as:

$$\begin{aligned}
&-\left[\left\{(E_cI_c)_{eq} + E_pI_p\right\} + I_p\tfrac{e_{311}^2}{a_{33}}\right]\left(\tfrac{h}{L^4}\right)\left[\tfrac{\partial^4W(X,t)}{\partial X^4}\right] \\
&\quad + \left(l^2\left[(E_cI_c)_{eq} - E_pI_p\right] + I_p\tfrac{\mu_{3111}^2}{a_{33}}\right)\left(\tfrac{h}{L^6}\right)\tfrac{\partial^6W(X,t)}{\partial X^6} \\
&\quad - \left(1 - \tfrac{(e_0a)^2}{L^2}\tfrac{\partial^2}{\partial X^2}\right)p(X) \\
&\quad = h\left[(\rho_cA_c)_{eq} + 2\rho_pA_p\right]\left[\tfrac{\partial^2W(X,t)}{\partial t^2} - \tfrac{(e_0a)^2}{L^2}\tfrac{\partial^4W(X,t)}{\partial X^2\partial t^2}\right] \\
&\quad - \left(\tfrac{h}{L^2}\right)\left[(\rho_cI_c)_{eq} + \rho_pI_p\right]\left[\tfrac{\partial^4W(X,t)}{\partial X^2\partial t^2} - \tfrac{(e_0a)^2}{L^2}\tfrac{\partial^6W(X,t)}{\partial X^4\partial t^2}\right]
\end{aligned} \tag{30}$$

Disregarding the nonlocality impact, motion equation of sandwich piezoelectric nanobeam with the microstructure effect will be:

$$\begin{aligned}
&-\left[\left\{(E_cI_c)_{eq} + E_pI_p\right\} + I_p\tfrac{e_{311}^2}{a_{33}}\right]\left(\tfrac{h}{L^4}\right)\left[\tfrac{\partial^4W(X,t)}{\partial X^4}\right] \\
&\quad + \left(l^2\left[(E_cI_c)_{eq} - E_pI_p\right] + I_p\tfrac{\mu_{3111}^2}{a_{33}}\right)\left(\tfrac{h}{L^6}\right)\tfrac{\partial^6W(X,t)}{\partial X^6} \\
&\quad - \left(1 - \tfrac{(e_0a)^2}{L^2}\tfrac{\partial^2}{\partial X^2}\right)\left(q(X,t) + \tfrac{hN_b}{L^2}\tfrac{\partial^2W(X,t)}{\partial X^2}\right. \\
&\quad \left. + \left[k_whW(X,t) - \tfrac{hk_p}{L^2}\tfrac{\partial^2W(X,t)}{\partial x^2}\right]\right) \\
&\quad = h\left[(\rho_cA_c)_{eq} + 2\rho_pA_p\right]\left[\tfrac{\partial^2W(X,t)}{\partial t^2}\right] \\
&\quad - \left(\tfrac{h}{L^2}\right)\left[(\rho_cI_c)_{eq} + \rho_pI_p\right]\left[\tfrac{\partial^4W(X,t)}{\partial X^2\partial t^2}\right]
\end{aligned} \tag{31}$$

Taking only the nonlocality effect, the equation of motion will be:

$$\begin{aligned}
&-\left[\left\{(E_cI_c)_{eq} + E_pI_p\right\} + I_p\tfrac{e_{311}^2}{a_{33}}\right]\left(\tfrac{h}{L^4}\right)\left[\tfrac{\partial^4W(X,t)}{\partial X^4}\right] + \left(I_p\tfrac{\mu_{3111}^2}{a_{33}}\right)\left(\tfrac{h}{L^6}\right)\tfrac{\partial^6W(X,t)}{\partial X^6} \\
&\quad - \left(1 - \tfrac{(e_0a)^2}{L^2}\tfrac{\partial^2}{\partial X^2}\right)\left(q(X,t) + \tfrac{hN_b}{L^2}\tfrac{\partial^2W(X,t)}{\partial X^2}\right. \\
&\quad \left. + \left[k_whW(X,t) - \tfrac{hk_p}{L^2}\tfrac{\partial^2W(X,t)}{\partial x^2}\right]\right) \\
&\quad = h\left[(\rho_cA_c)_{eq} + 2\rho_pA_p\right]\left[\tfrac{\partial^2W}{\partial t^2} - \tfrac{(e_0a)^2}{L^2}\tfrac{\partial^4W(X,t)}{\partial X^2\partial t^2}\right] \\
&\quad - \left(\tfrac{h}{L^2}\right)\left[(\rho_cI_c)_{eq} + \rho_pI_p\right]\left[\tfrac{\partial^4W}{\partial X^2\partial t^2} - \tfrac{(e_0a)^2}{L^2}\tfrac{\partial^6W(X,t)}{\partial X^4\partial t^2}\right]
\end{aligned} \tag{32}$$

Ignoring the nonclassical effects, results the classical equation of motion as:

$$
\begin{aligned}
&-\left[\left\{(E_cI_c)_{eq}+E_pI_p\right\}+I_p\frac{e_{311}^2}{a_{33}}\right]\left(\frac{h}{L^4}\right)\left[\frac{\partial^4W(X,t)}{\partial X^4}\right]+\left(I_p\frac{\mu_{3111}^2}{a_{33}}\right)\left(\frac{h}{L^6}\right)\frac{\partial^6W(X,t)}{\partial X^6}\\
&\qquad-\left(q(x,t)+\frac{hN_b}{L^2}\frac{\partial^2W(X,t)}{\partial X^2}\right.\\
&\qquad\left.+\left[k_whW(x,t)-\frac{hk_p}{L^2}\frac{\partial^2W(X,t)}{\partial x^2}\right]\right)\\
&\qquad=h\left[(\rho_cA_c)_{eq}+2\rho_pA_p\right]\left[\frac{\partial^2W(X,t)}{\partial t^2}\right]\\
&\qquad-\left(\frac{h}{L^2}\right)\left[(\rho_cI_c)_{eq}+\rho_pI_p\right]\left[\frac{\partial^4W(X,t)}{\partial X^2\partial t^2}\right]
\end{aligned}
\tag{33}
$$

Neglecting the flexoelectric, piezoelectric, and the nonclassical effects leads to the classical equation of motion of perforated beam as:

$$
\begin{aligned}
&-(E_cI_c)_{eq}\left(\frac{h}{L^4}\right)\left[\frac{\partial^4W(X,t)}{\partial X^4}\right]\\
&\qquad-\left(q(x,t)+\frac{hN_b}{L^2}\frac{\partial^2W(X,t)}{\partial X^2}\right.\\
&\qquad\left.+\left[k_whW(x,t)-\frac{hk_p}{L^2}\frac{\partial^2W(X,t)}{\partial x^2}\right]\right)\\
&\qquad=h\left[(\rho_cA_c)_{eq}\right]\left[\frac{\partial^2W(X,t)}{\partial t^2}\right]-\left(\frac{h}{L^2}\right)\left[(\rho_cI_c)_{eq}\right]\left[\frac{\partial^4W(X,t)}{\partial X^2\partial t^2}\right]
\end{aligned}
\tag{34}
$$

4. Analytical Solution Methodology

Within this section, analytical solutions for the size-dependent electromechanical free vibration behavior of composite nanobeams with a perforated core and piezoelectric face sheets are proposed. Neglecting the applied external loadings, the nonclassical electromechanical dynamic equation of motion could be written as:

$$
\begin{aligned}
&\left[\left\{(E_cI_c)_{eq}+E_pI_p\right\}+I_p\frac{e_{311}^2}{a_{33}}\right]\left(\frac{h}{L^4}\right)\left[\frac{\partial^4W(X,t)}{\partial X^4}\right]\\
&\qquad+\left(l^2\left[(E_cI_c)_{eq}-E_pI_p\right]+I_p\frac{\mu_{3111}^2}{a_{33}}\right)\left(\frac{h}{L^6}\right)\frac{\partial^6W(X,t)}{\partial X^6}\\
&\qquad-\left[k_whW(x,t)-\frac{hk_p}{L^2}\frac{\partial^2W(X,t)}{\partial x^2}\right]\\
&\qquad+\left(\frac{(e_0a)^2}{L^2}\right)\left[k_wh\frac{\partial^2W(x,t)}{\partial X^2}-\frac{hk_p}{L^2}\frac{\partial^4W(X,t)}{\partial x^4}\right]\\
&\qquad=h\left[(\rho_cA_c)_{eq}+2\rho_pA_p\right]\left[\frac{\partial^2W(X,t)}{\partial t^2}-\frac{(e_0a)^2}{L^2}\frac{\partial^4W(X,t)}{\partial X^2\partial t^2}\right]\\
&\qquad-\left(\frac{h}{L^2}\right)\left[(\rho_cI_c)_{eq}+\rho_pI_p\right]\left[\frac{\partial^4W(X,t)}{\partial X^2\partial t^2}-\frac{(e_0a)^2}{L^2}\frac{\partial^6W(X,t)}{\partial X^4\partial t^2}\right]
\end{aligned}
\tag{35}
$$

Assume that the solution of Equation (35) is given in the following form [47]:

$$
W=\sum_{n=1}^{\infty}W_n\Phi_n(X)e^{i\omega_nt}
\tag{36}
$$

where, W_n, $\Phi_n(X)$, respectively, refer to the unknown variable and mode shape function that satisfy the boundary conditions (BCs), $i^2 = -1$, ω_n denotes to vibration frequency for each mode, for simply supported beam, $\Phi_n(X) = \sin(n\pi X)$.

$$\left\{\begin{matrix} \frac{\partial^2 W(X,t)}{\partial X^2} & \frac{\partial^2 W(X,t)}{\partial t^2} \\ \frac{\partial^4 W(X,t)}{\partial X^4} & \frac{\partial^4 W(X,t)}{\partial X^2 \partial t^2} \\ \frac{\partial^6 W(X,t)}{\partial X^6} & \frac{\partial^6 W(X,t)}{\partial X^4 \partial t^2} \end{matrix}\right\} = \sum_{n=1}^{\infty}\left(\left\{\begin{matrix} -(n\pi)^2 & -(\omega_n)^2 \\ (n\pi)^4 & (n\pi)^2(\omega_n)^2 \\ -\sum\limits_{n=1}^{\infty}(n\pi)^6 & -(n\pi)^4(\omega_n)^2 \end{matrix}\right\} W_n \sin(n\pi X) e^{i\omega_n t}\right) \tag{37}$$

Substituting Equations (36) and (37) into Equation (35) yields:

$$\begin{aligned} &\left[\sum_{n=1}^{\infty}\left\{\left[\left\{(E_c I_c)_{eq} + E_p I_p\right\} + I_p \frac{e_{311}^2}{a_{33}}\right]\left(\frac{h}{L^4}\right)(n\pi)^4\right.\right. \\ &\quad + \left(l^2\left[(E_c I_c)_{eq} - E_p I_p\right] + I_p \frac{\mu_{3111}^2}{a_{33}}\right)\left(\frac{h}{L^6}\right)(n\pi)^6 \\ &\quad + \left(k_w h + \left(\frac{hk_p}{L^2}\right)(n\pi)^2\right)(1 \\ &\quad \left.\left. + \frac{(e_0 a)^2}{L^2}(n\pi)^2\right)\right\} W_n \sin(n\pi X) e^{i\omega_n t}\Big] \\ &\quad = (\omega_n)^2\left[\left(\sum_{n=1}^{\infty}\left\{h\left[(\rho_c A_c)_{eq} + 2\rho_p A_p\right]\left(1 + \frac{(e_0 a)^2}{L^2}(n\pi)^2\right)\right.\right.\right. \\ &\quad + \left(\frac{h}{L^2}\right)\left[(\rho_c I_c)_{eq} + \rho_p I_p\right](n\pi)^2(1 \\ &\quad \left.\left.\left. + \frac{(e_0 a)^2}{L^2}(n\pi)^2\right)\right\} W_n \sin(n\pi X) e^{i\omega_n t}\right)\right] \end{aligned} \tag{38}$$

The nonclassical electromechanical resonant frequencies could be expressed as:

$$\begin{aligned} &\left(\omega_n^{NELEM}\right)^2 \\ &= \frac{\left[\left\{(E_c I_c)_{eq} + E_p I_p\right\} + I_p \frac{e_{311}^2}{a_{33}}\right]\left(\frac{n\pi}{L}\right)^4 + \left(l^2\left[(E_c I_c)_{eq} + E_p I_p\right] + I_p \frac{\mu_{3111}^2}{a_{33}}\right)\left(\frac{n\pi}{L}\right)^6 + \left(k_w + \left(\frac{k_p}{L^2}\right)(n\pi)^2\right)\left(1 + (e_0 a)^2\left(\frac{n\pi}{L}\right)^2\right)}{\left(1 + (e_0 a)^2\left(\frac{n\pi}{L}\right)^2\right)\left\{\left[(\rho_c A_c)_{eq} + 2\rho_p A_p\right] + \left[(\rho_c I_c)_{eq} + \rho_p I_p\right]\left(\frac{n\pi}{L}\right)^2\right\}} \end{aligned} \tag{39}$$

Neglecting the nonclassical effects, the classical resonant frequency could be given by:

$$\begin{aligned} &\left(\omega_n^{CELEM}\right)^2 \\ &= \frac{\left[\left\{(E_c I_c)_{eq} + E_p I_p\right\} + I_p \frac{e_{311}^2}{a_{33}}\right]\left(\frac{n\pi}{L}\right)^4 + \left(I_p \frac{\mu_{3111}^2}{a_{33}}\right)\left(\frac{n\pi}{L}\right)^6 + \left(k_w + \left(\frac{k_p}{L^2}\right)(n\pi)^2\right)}{\left\{\left[(\rho_c A_c)_{eq} + 2\rho_p A_p\right] + \left[(\rho_c I_c)_{eq} + \rho_p I_p\right]\left(\frac{n\pi}{L}\right)^2\right\}} \end{aligned} \tag{40}$$

Neglecting the piezoelectric and flexoelectric effects, the nonclassical mechanical frequency could be written as:

$$\begin{aligned} &\left(\omega_n^{NMEC}\right)^2 \\ &= \frac{(E_c I_c)_{eq}\left(\frac{n\pi}{L}\right)^4 + l^2\left[(E_c I_c)_{eq}\right]\left(\frac{n\pi}{L}\right)^6 + \left(k_w + \left(\frac{k_p}{L^2}\right)(n\pi)^2\right)\left(1 + (e_0 a)^2\left(\frac{n\pi}{L}\right)^2\right)}{\left(1 + (e_0 a)^2\left(\frac{n\pi}{L}\right)^2\right)\left\{\left[(\rho_c A_c)_{eq}\right] + \left[(\rho_c I_c)_{eq}\right]\left(\frac{n\pi}{L}\right)^2\right\}} \end{aligned} \tag{41}$$

Neglecting the piezoelectric, flexoelectric as well as nonclassical effects, the classical mechanical frequency could be written as:

$$\left(\omega_n^{CMEC}\right)^2 = \frac{(E_c I_c)_{eq}\left(\frac{n\pi}{L}\right)^4 + \left(k_w + \left(\frac{k_p}{L^2}\right)(n\pi)^2\right)}{\left\{\left[(\rho_c A_c)_{eq}\right] + \left[(\rho_c I_c)_{eq}\right]\left(\frac{n\pi}{L}\right)^2\right\}} \tag{42}$$

Considering the other BCs, for clamped-clamped (CC) BCs are:

$$W = \frac{\partial W}{\partial X} = 0 \ \ at \ X = 0 \ and \ X = 1 \tag{43}$$

While the mode shape function, $\Phi_n(X)$ is expressed as:

$$\begin{gathered}\Phi_n(X) = \cosh(k_n X) - \cos(k_n X) - \beta_n[\sinh(k_n X) - \sin(k_n X)], \\ \beta_n = \frac{\cosh(k_n) - \cos(k_n)}{\sinh(k_n) - \sin(k_n)}\ , \text{ and } \ \cos(k_n)\cosh(k_n) = 1\end{gathered} \tag{44}$$

On the other hand, for clamped-free (CF) BCs are given as:

$$W = \frac{\partial W}{\partial X} = 0 \ \ at \ X = 0 \text{ and } \ \frac{\partial^2 W}{\partial X^2} = \frac{\partial^3 W}{\partial X^3} = 0 \ \text{ at } X = 1 \tag{45}$$

While the mode shape function, $\Phi_n(X)$ is expressed as:

$$\begin{gathered}\Phi_n(X) = \cosh(k_n X) - \cos(k_n X) - \beta_n[\sinh(k_n X) - \sin(k_n X)], \\ \beta_n = \frac{\cosh(k_n) + \cos(k_n)}{\sinh(k_n) + \sin(k_n)}\ , \text{ and } \ \cos(k_n)\cosh(k_n) = -1\end{gathered} \tag{46}$$

Additionally, for clamped-simple (CS) configuration, the boundary conditions are given as:

$$W = \frac{\partial W}{\partial X} = 0 \ \ at \ X = 0 \text{ and } \ \frac{\partial^2 W}{\partial X^2} = W = 0 \ \text{ at } X = 1 \tag{47}$$

While the mode shape function, $\Phi_n(X)$ is expressed as:

$$\begin{gathered}\Phi_n(X) = \cosh(k_n X) - \cos(k_n X) - \beta_n[\sinh(k_n X) - \sin(k_n X)], \\ \beta_n = \frac{\cosh(k_n) - \cos(k_n)}{\sinh(k_n) - \sin(k_n)}\ , \text{ and } \ \tan(k_n) = \tanh(k_n)\end{gathered} \tag{48}$$

Applying the Galerken's procedure, the resonant frequencies for CC, CF, and CS beam configurations could be expressed as:

$$\begin{aligned}&\left(\omega_n^{NELEM}\right)^2 \\ &= \frac{\left[\left\{(E_c I_c)_{eq} + E_p I_p\right\} + I_p \frac{e_{311}^2}{a_{33}}\right]\left(\frac{k_n}{L}\right)^4 + \left(l^2\left[(E_c I_c)_{eq} + E_p I_p\right] + I_p \frac{\mu_{3111}^2}{a_{33}}\right)\left(\frac{k_n}{L}\right)^6 (\xi_n) + \left(k_w + k_p \xi_n \left(\frac{k_n}{L}\right)^2\right)\left(1 + (e_0 a)^2 \left(\frac{k_n}{L}\right)^2 (\xi_n)\right)}{\left(1 + (e_0 a)^2\left(\frac{k_n}{L}\right)^2 (\xi_n)\right)\left(\left[(\rho_c A_c)_{eq} + 2\rho_p A_p\right] + \left[(\rho_c I_c)_{eq} + \rho_p I_p\right]\left(\frac{k_n}{L}\right)^2 (\xi_n)\right)}\end{aligned} \tag{49}$$

where ξ_n is given by:

$$\begin{aligned}\xi_n = \int_0^1 \{&(\cosh(k_n) + \cos(k_n)) \\ &-\beta_n(\sinh(k_n X) + \sin(k_n X))\}\{(\cosh(k_n) - \cos(k_n)) \\ &-\beta_n(\sinh(k_n X) - \sin(k_n X))\}dX\end{aligned} \tag{50}$$

where k_n, β_n, and ξ_n are numerically evaluated for the different vibration modes, Zeng et al. [42].

5. Numerical Results and Discussion

Within this section, the proposed analytical procedure is first verified to check the numerical efficiency. Numerical experiments are performed to explore the influences of the design variables on the nonclassical electromechanical dynamic behavior of composite nanobeams embedded in an elastic foundation.

5.1. Verification of the Developed Methodology for Free Vibration Analysis

To prove the accuracy of the analytical technique in investigating the piezoelectric vibration response of the composite beam structure, consider a simply supported (SS) composite beam macro having the following material and geometrical parameters: the elastic core modulus (E_c = 130 MPa), the piezoelectric modulus (E_p = 32 GPa), and the core mass density (ρ_c = 126 kg/m^3) of the piezoelectric density (ρ_p = 1380 kg/m^3). A beam length of L = 1.2 m, h_c = 10 mm is the core thickness, h_p = 0.5 mm is the piezoelectric thickness, and h_t = 11 mm is the overall beam thickness. The same problem is previously analyzed analytically by Zeng et al. [42] and Chanthanumataporn and Watanabe [48] and numerically using the finite element (FE) analysis by Chanthanumataporn and Watanabe [48]. Neglecting the piezoelectricity as well as the size-dependent effects, a comparison of the obtained classical circular frequencies for the first lowest eight modes with those found in the literature is illustrated in Figure 2. It can be observed that there is an excellent agreement with the published results, especially for analytical solutions.

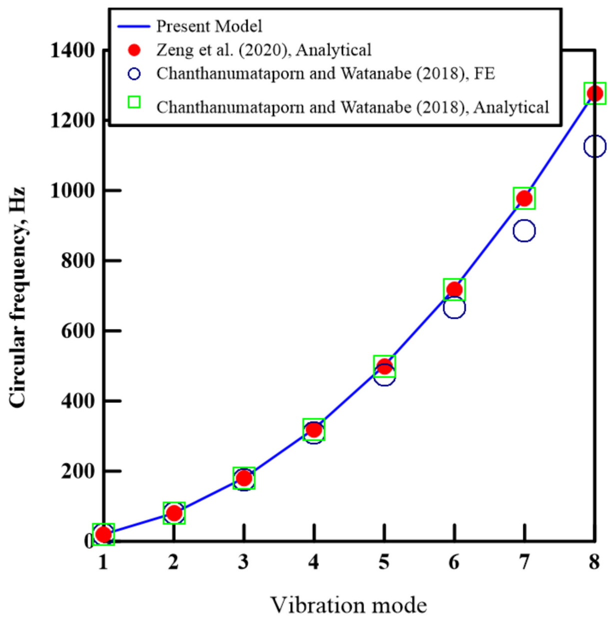

Figure 2. Variation in the classical mechanical circular frequencies with vibration modes of simply-simply (SS) supported composite beam for, $l/h = ea/h$ = 0 nm, and $\nu_c = \nu_p = = k_w = k_p = 0$ [42,48].

Seeking for deeper verification of the proposed analytical methodology to efficiently examine a nonclassical electromechanical vibration response of sandwich nanobeam structures, we considered the following geometrical parameters of piezoelectric composite beam: the elastic core thickness, h_c = 0, the overall beam thickness, h_t = 2 nm, the thickness of each piezoelectric face layer, h_p = 1 nm. The Young's modulus of the piezoelectric layer E_p = 132 GPa and the mass density, ρ_p = 7500 kg/m^3 were utilized. The piezoelectric parameters are given as: $e_{311} = -4.1$ C/m^2, $a_{33} = 7.124 \times 10^{-9}$ N/(m^2.K). The nondimensional nonlocal parameter is given as (ea/L) = 0.1, the nondimensional strain gradient parameter as (l/L) = 0, and the perforation parameter as α = 1. The problem was considered previously by Ke et al. [49] and Zeng et al. [42]. The nondimensional frequency is evaluated by $\lambda_1 = \omega_{n1} L\sqrt{\frac{\rho_p}{E_p}}$. The nondimensional foundation parameters are expressed as $K_w = \frac{k_w L^4}{E_p I_p}$ and $K_p = \frac{k_w L^2}{E_p I_p}$. Comparison of λ_1 for the piezoelectric nanobeam at different beam aspect ratios, L/h_t and nondimensional elastic foundation parameters, K_w at K_p = 0 for various BCs is shown in Table 1. It observed a good agreement between the obtained results and that obtained by Ke et al. [49] and Zeng et al. [42].

Table 1. Variations in the nonclassical fundamental electromechanical frequency parameter, $\lambda_1 = \omega_{n1} L \sqrt{\frac{\rho_p}{E_p}}$, at different values of the nondimensional elastic foundation parameter, K_w, and beam slenderness ratio for different BCS for $(l/L) = 0$ $a_{33} = 7.124 \times 10^{-9}$ N/(m^2.K), $(ea/L) = 0.1$, $K_p = 0$, $\alpha = 1$.

L/h_t	K_w	SS			CC		CS			CF	
		Present	**Ref [49]**	**Ref [44]**	**Present**	**Ref [44]**	**Present**	**Ref [49]**	**Ref [44]**	**Present**	**Ref [44]**
6	0	0.4519	0.4570	0.4571	1.0149	1.0245	0.7012	0.7077	0.7087	0.1699	0.1714
	10^2	0.6562	--------	--------	--------	--------	0.8454	--------	--------	0.5098	--------
	10^4	4.7786	--------	--------	--------	--------	4.7996	--------	--------	4.8095	--------
8	0	0.3406	0.3428	0.3428	0.7644	0.7684	0.5284	0.5310	0.5315	0.1274	0.1285
	10^2	0.4945	--------	--------	0.8424	--------	0.6377	--------	--------	0.3825	--------
	10^4	3.6016	--------	--------	3.6602	--------	3.6203	--------	--------	3.6087	--------
10	0	0.2731	0.2742	0.2742	0.6127	0.6167	0.4236	0.4250	0.4252	0.1020	0.1028
	10^2	0.3965	--------	--------	0.6758	--------	0.5115	--------	--------	0.306	--------
	10^4	2.8879	--------	--------	2.9365	--------	2.904	--------	--------	2.8875	--------
16	0	0.1711	0.1714	0.1714	0.3838	0.3842	0.2654	0.2658	0.2658	0.0637	0.0643
	10^2	0.2485	--------	--------	0.4237	--------	0.3206	--------	--------	0.1913	--------
	10^4	1.8094	--------	--------	1.841	--------	1.8203	--------	--------	1.8051	--------
20	0	0.1370	0.1371	0.1371	0.3072	0.3073	0.2124	0.2127	0.2126	0.0510	0.0514
	10^2	0.1989	-------	--------	0.3392	--------	0.2567	--------	--------	0.1531	--------
	10^4	1.4484	-------	--------	1.4739	--------	1.4572	--------	--------	1.4441	--------
30	0	0.0914	0.0914	0.0914	0.2049	0.2049	0.1417	0.1420	0.1417	0.0340	0.0343
	10^2	0.1327	-------	--------	0.2263	--------	0.1712	--------	--------	0.102	--------
	10^4	0.9661	-------	--------	0.9833	--------	0.9721	--------	--------	0.9628	--------

Another verification of the developed methodology is performed to check the accuracy of the analytical procedure to efficiently investigate the vibration response of the beam structure. For this comparison, the following nondimensional frequency parameter is defined: $\sqrt{\lambda_1} = \left(\frac{\omega_{n1}^2 L^4 \rho A}{E_{eq} I}\right)^{\frac{1}{4}}$ where E_{eq} is the equivalent elasticity modulus, which can be expressed as $E_{eq} = \lambda + 2G$; where λ is the Lame's constant, $\lambda = \frac{\nu E}{(1+\nu)(1-2\nu)}$ and G is the rigidity modulus, $G = \frac{E}{2(1+\nu)}$. The nondimensional elastic foundation parameters are defined as $K_w = \frac{k_w L^4}{E_{eq} I}$ and $\frac{K_p}{\pi^2} = \frac{k_w L^2}{E_{eq} I \pi^2}$. Comparisons of the fundamental nondimensional frequency parameter $\sqrt{\lambda_1}$ for the simply supported beam (SS) for different values of the nondimensional elastic foundation parameters, K_w and K_p and for beam aspect ratios, $L/H = 15$ and 120, which are depicted in Table 2. It is observed that excellent agreement with results reported by Chen et al. [50] and De Rosa and Maurizi [51] verifies the proposed methodology.

Table 2. Variations in the classical electromechanical fundamental nondimensional frequency parameter $\sqrt{\lambda_1}$ for simply supported (SS) beam embedded in two parameters elastic foundation at beam aspect ratio L/h_t = 120 at different values of the elastic foundation parameters.

Foundation Parameters		$\sqrt{\lambda_1}=\left(\frac{\omega_{n1}^2 L^4 \rho A}{E_{eq} I}\right)^{\frac{1}{4}}$ **for** L/H **= 120**					$\sqrt{\lambda_1}=\left(\frac{\omega_{n1}^2 L^4 \rho A}{E_{eq} I}\right)^{\frac{1}{4}}$ **for** L/H **= 15**			
K_w	$\frac{K_p}{\pi^2}$	**Present**	**Ref [50]**	**Analytical, Ref [50]**	**Ref [51]**	**% Error**	**Present**	**Ref [50]**	**Analytical, Ref [50]**	**% Error**
0	0	3.141548	3.141434	3.141417	3.1415	0.0042	3.1387282	3.1302472	3.1302475	0.270927
	0.5	3.476694	3.476594	3.476589	3.4767	0.0030	3.4735738	3.4667120	3.4667123	0.197925
	1.0	3.735951	3.735876	3.735859	3.7360	0.0025	3.732598	3.7265663	3.7265663	0.161857
	2.5	4.296954	4.296866	4.296879	4.2970	0.0017	4.2930972	4.2880927	4.2880929	0.116702
10^2	0	3.748311	3.748233	3.748219	3.7483	0.0025	3.7449466	3.7389476	3.7389477	0.160444
	0.5	3.960753	3.960677	3.960669	3.9608	0.0021	3.9571978	3.9516805	3.9516807	0.139614
	1.0	4.143643	4.143563	4.143565	4.1437	0.0019	4.1399244	4.1347186	4.1347188	0.12590
	2.5	4.582333	4.582266	4.582264	4.5824	0.0015	4.5782205	4.5734720	4.5734720	0.103827
10^4	0	10.024121	10.02403	10.02404	10.024	0.0008	10.015124	9.9958218	9.9958219	0.193102
	0.5	10.036187	10.03610	10.03610	10.036	0.0009	10.0271791	10.007782	10.007782	0.19382
	1.0	10.048209	10.04813	10.04813	10.048	0.0008	10.0391909	10.019699	10.019699	0.194536
	2.5	10.08402	10.08394	10.08394	10.084	0.0008	10.07497	10.055193	10.055193	0.196684

Comparisons of the frequency parameter for the lowest three vibration modes for the clamped-clamped (CC) beam at different values of the nondimensional frequency parameters for L/H = 15 and 120 are illustrated in Table 3. It is noticeable that there is good agreement with the results obtained by Chen et al. [50] and De Rosa and Maurizi [51].

5.2. Parametric Studies

Within this section, parametric studies are performed to explore the effects of geometrical as well as material characteristics on the nonclassical electromechanical dynamic behavior of piezoelectrically layered perforated nanobeams embedded in two variables of an elastic foundation. To conduct this, we considered a composite beam structure composed of a regularly perforated elastic core and two piezoelectric face sheet layers. Both material and geometrical properties of the composite beam structures are shown in Table 4, otherwise stated by Zeng et al. [42]. The nondimensional electromechanical frequency parameter, $\lambda_{ni}^{Elec} = \omega_{ni}^{Elec} L^2 \sqrt{\frac{[(\rho A)_c]_{eq} + 2(\rho A)_p}{\left[(E_{eq} I)_c\right]_{eq} + (E_{eq} I)_p}}$, and the nondimensional mechanical frequency parameter, $\lambda_{ni}^{Mec} = \omega_{ni}^{Mec} L^2 \sqrt{\frac{(\rho A)_{eq}}{(E_{eq} I)_{eq}}}$, with n refers to the vibration mode. The nondimensional elastic foundation parameters for the piezoelectric composite beam are defined as follows: $K_w^{Elect} = \frac{k_w L^4}{(E_{eq} I)_c + (E_{eq} I)_p}$ and $\frac{K_p^{Elect}}{\pi^2} = \frac{k_p L^2}{\left((E_{eq} I)_c + (E_{eq} I)_p\right)\pi^2}$. The homogeneous perforated beam could be expressed as $K_w^{EMec} = \frac{k_w L^4}{(E_{eq} I)}$ and $\frac{K_p^{Elect}}{\pi^2} = \frac{k_p L^2}{(E_{eq} I)\pi^2}$.

Table 3. Comparison of the estimated classical fundamental nondimensional frequency parameter $\sqrt{\lambda_1}$ for clamped-clamped (CC) beam embedded in two parameters elastic foundation at beam aspect ratio L/h = 120 at different values of the elastic foundation parameters for α = 1.

Foundation Parameters		$\sqrt{\lambda_n}=\left(\frac{\omega_n^2 L^4 \rho A}{E_{eq} I}\right)^{\frac{1}{4}}$ for $L/H = 120$								
		$\sqrt{\lambda_1}$			$\sqrt{\lambda_2}$			$\sqrt{\lambda_3}$		
K_w	$\frac{K_p}{\pi^2}$	Present	Ref [50]	Ref [51]	Present	Ref [50]	Ref [51]	Present	Ref [50]	Ref [51]
0	0	4.7299	4.7314	4.73	7.8527	7.8533	7.854	10.9940	10.9908	10.996
	0.5	4.8672	4.8683	4.869	7.9674	7.9680	7.968	11.0847	11.0815	11.086
	1.0	4.9938	4.9938	4.994	8.0774	8.0777	8.078	11.1732	11.1700	11.174
	2.5	5.3250	5.3195	5.32	8.3830	8.3812	8.38	11.4267	11.4233	11.43
10^2	0	4.9503	4.9515	4.95	7.9038	7.904	7.904	11.0128	11.0096	11.014
	0.5	5.0709	5.0718	5.071	8.0164	8.0169	8.017	11.1030	11.0998	11.104
	1.0	5.1835	5.1834	5.182	8.1244	8.1247	8.124	11.1910	11.1878	11.192
	2.5	5.4834	5.4783	5.477	8.4251	8.4234	8.423	11.4434	11.4400	11.444
10^4	0	10.1227	10.1227	10.123	10.8385	10.8384	10.839	12.5242	12.5216	12.526
	0.5	10.1373	10.1373	10.137	10.8828	10.8827	10.883	12.5858	12.5832	12.588
	1.0	10.1518	10.1517	10.152	10.9266	10.9264	10.927	12.6465	12.6439	12.648
	2.5	10.1951	10.1942	10.194	11.0550	11.0539	11.055	12.8237	12.8209	12.825
		$\sqrt{\lambda_n}=\left(\frac{\omega_n^2 L^4 \rho A}{E_{eq} I}\right)^{\frac{1}{4}}$ for $L/H = 15$								
0	0	4.7246271	4.66554	-----	7.8200665	7.61037	-----	10.8971419	10.42711	-----
	0.5	4.8618011	4.80385	-----	7.9343451	7.72927	-----	10.9869929	10.52435	-----
	1.0	4.9882582	4.93027	-----	8.0438889	7.84259	-----	11.0746921	10.61889	-----
	2.5	5.3190604	5.25671	-----	8.3481637	8.15441	-----	11.3259972	10.88791	-----
10^2	0	4.9447357	4.89268	-----	7.8709675	7.66521	-----	10.9157313	10.44810	-----
	0.5	5.0652311	5.01352	-----	7.9831048	7.78165	-----	11.0051315	10.54476	-----
	1.0	5.1776934	5.12542	-----	8.0907063	7.89277	-----	11.0924046	10.63876	-----
	2.5	5.4772355	5.41981	-----	8.3900963	8.19912	-----	11.3425599	10.90635	-----
10^4	0	10.1113553	10.04899	-----	10.7934756	10.70252	-----	12.4138087	12.08187	-----
	0.5	10.1259392	10.0640	-----	10.8376283	10.7461	-----	12.4748902	12.14487	-----
	1.0	10.1404604	10.07881	-----	10.8812478	10.78903	-----	12.5350874	12.20684	-----
	2.5	10.1836536	10.12225	-----	11.0090521	10.91414	-----	12.710659	12.38693	-----

Table 4. The geometric and material constants of the piezoelectrically layered composite nanobeam.

Parameters	Thickness (nm)	Length (nm)	Width (nm)	Young's Modulus (GPa)	Mass Density (Kg/m^3)	Poisson's Ratio	e_{311} (C/m^2)	μ_{3111} (C/m)	a_{33} N/(m^2.K)	l
Elastic core	3	100	5	0.130	1380	0.24	----	----	-----	h
Piezoelectric Layer	1	100	5	132	7500	0.27	-4.1	5×10^{-8}	7.124×10^{-9}	h

5.2.1. Effect of the Nondimensional Elastic Foundation Parameters, K_w and K_p

Neglecting the effect of the shear component of the elastic foundation parameter, K_p, the dependency of the resonant frequency parameters of the first lowest three vibration modes on the nondimensional elastic foundation parameter, K_w, for both nonclassical and classical electromechanical and mechanical behaviors at different values of the material Poisson's ratio for different composite nanobeam BCS are depicted in Figure 3. It is noticed that for both electromechanical and mechanical nonclassical and classical behaviors, the fundamental resonant frequency parameter, λ_1, increases with increasing the nondimensional foundation parameter, K_w, due to increasing the overall system stiffness. This effect becomes insignificant as the vibration modes proceed; almost constant behaviors are observed at the third vibration mode. Additionally, neglecting the effect of the material Poisson's ratio leads to underestimates of the nondimensional frequency parameters for all behaviors and beam BCs; smaller values are obtained compared with the corresponding cases obtained by considering Poisson's ratio effect. Moreover, the incorporation of the flexoelectric and piezoelectricity effects leads to larger values of the nondimensional frequency parameters compared with the corresponding mechanical behavior, especially at smaller values of elastic foundation stiffness. Increasing the elastic foundation parameter, K_w, may produce larger values of the mechanical nondimensional frequency parameters compared with the corresponding electromechanical behavior, especially at the first vibration mode. Incorporating the nonclassical effect with $(l/h) < (ea/h)$ leads to smaller values of the nondimensional frequency parameters compared with the corresponding classical behaviors due to the associated softening effect. Comparing the corresponding BCs, the CC configuration produces the largest values of the nondimensional fundamental frequency parameters, while the CF results in the smallest values.

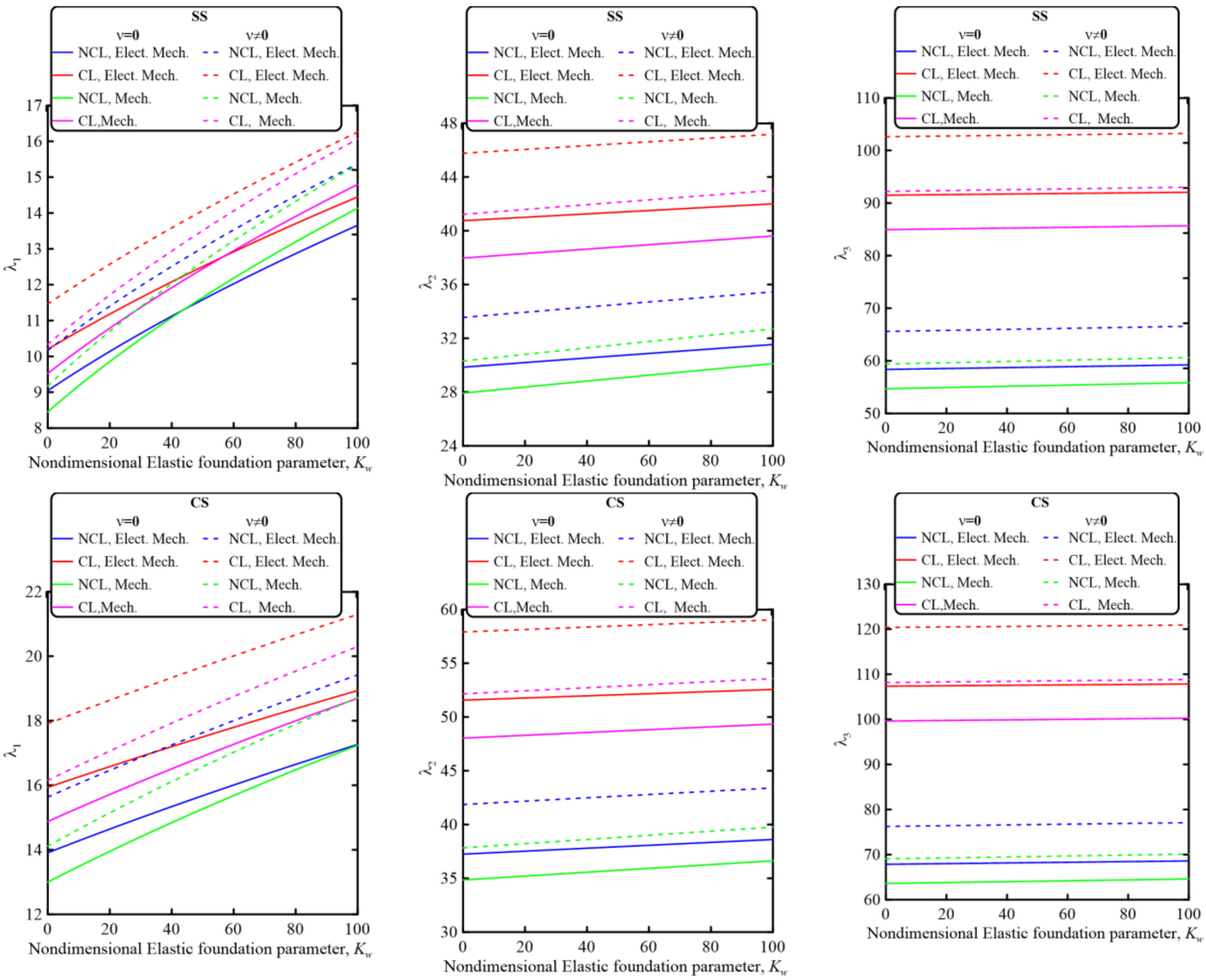

Figure 3. *Cont.*

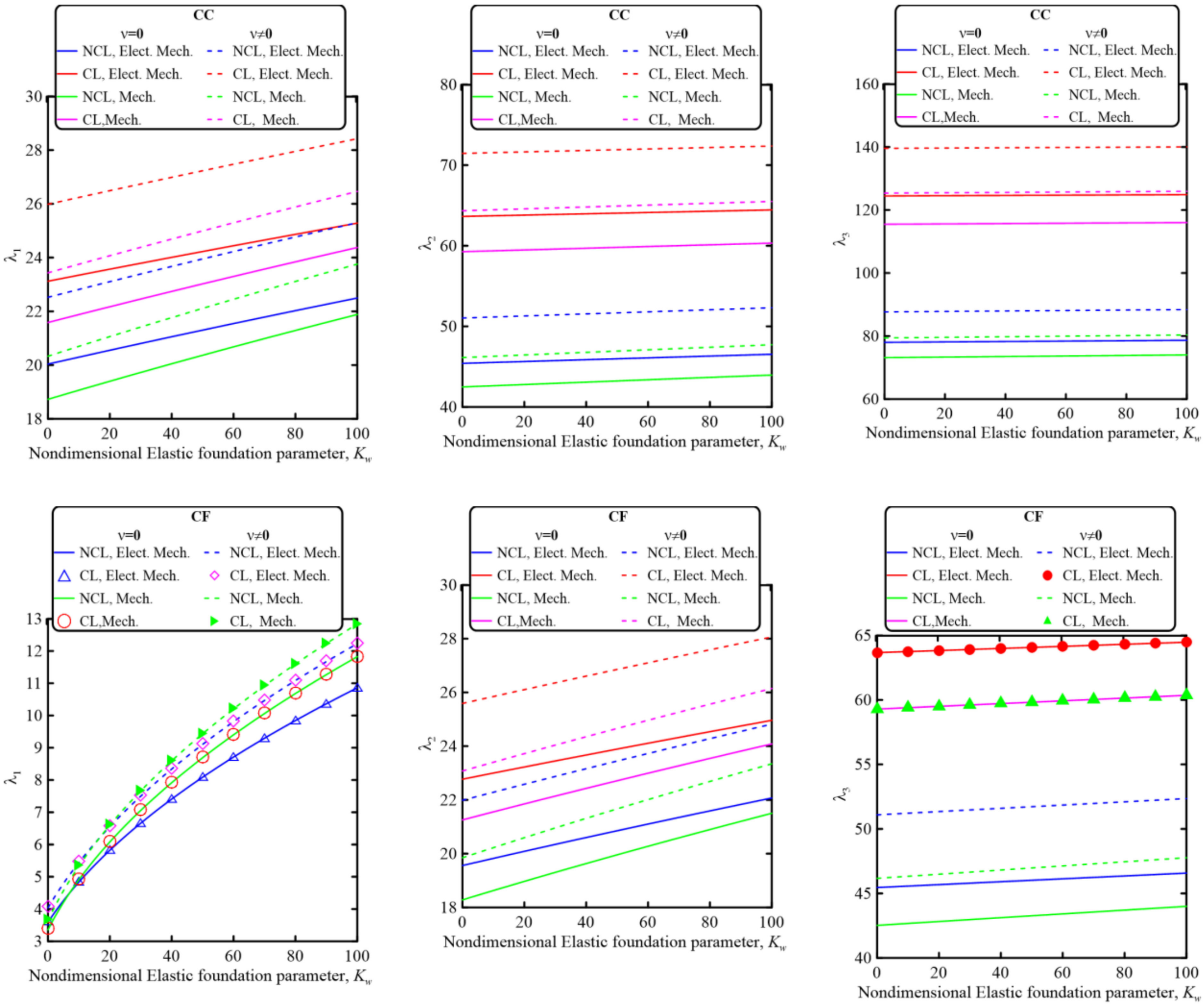

Figure 3. Dependency of the fundamental resonant frequency parameters of the lowest three vibration modes on the nondimensional foundation parameter, K_w, at different values of material Poisson's ratio, ν, for different nonclassical and classical behaviors of piezoelectric composite nanobeams for different BCs, at N = 4 and beam aspect ratio, L/h = 20, e_0a/h = 4, l/h = 2, α = 0.5, and K_p = 0, ν_c = 0.24, ν_p = 0.27.

To explore the effect of considering the material Poisson's ratio, Table 5 shows the variations of the nondimensional frequency parameters for the first lowest three vibration modes of the nonclassical electromechanical and mechanical behaviors for CC and CF BCs. The relative percentage difference is defined as $\%E = 100 \times \left(\frac{\lambda_i^{\nu\neq0} - \lambda_i^{\nu=0}}{\lambda_i^{\nu=0}}\right)$. It is clear that considering the material Poisson's ratio has significant effects in detecting the nondimensional frequency parameters. The relative percentage difference reaches 12.5% for the electromechanical behavior, while for the mechanical behavior, this relative percentage difference reaches about 8.6%.

Table 5. Effect of the material Poisson's ratio on the frequency parameters of the first three vibration modes for electromechanical and mechanical nonclassical behaviors for CC and CF BCs at different values of the nondimensional elastic foundation parameter, K_w, for N = 4 and beam aspect ratio, L/h = 20, e_0a/h = 4, l/h = 2, α = 0.5, and K_p = 0, ν_c = 0.24, ν_p = 0.27.

K_w	CC						CF					
	NCL_Elect		%E	NCL_Mech		%E	NCL_Elect		%E	NCL_Mech		%E
	$\nu = 0$	$\nu \neq 0$		$\nu = 0$	$\nu \neq 0$		$\nu = 0$	$\nu \neq 0$		$\nu = 0$	$\nu \neq 0$	
							λ_1					
0	20.0360	22.5228	12.4117	18.7259	20.3300	8.5662	3.5897	4.0356	12.4217	3.3542	3.6415	8.5654
5	20.1661	22.6696	12.4144	18.8963	20.5150	8.5662	4.2587	4.7903	12.4827	4.2045	4.5647	8.5670
25	20.6783	23.2476	12.4251	19.5630	21.2388	8.5662	6.2562	7.0421	12.5619	6.5869	7.1511	8.5655
50	21.3012	23.9504	12.4369	20.3657	22.1102	8.5659	8.0867	9.1048	12.5898	8.6904	9.4348	8.5658
100	22.4953	25.2976	12.4573	21.8829	23.7574	8.5660	10.8583	12.2274	12.6088	11.8235	12.8364	8.5668
							λ_2					
0	45.4108	51.0377	12.3911	42.4857	46.1251	8.5662	19.5591	21.9865	12.4106	18.2806	19.8466	8.5665
5	45.4677	51.1019	12.3917	42.5605	46.2063	8.5662	19.6923	22.1369	12.4140	18.4551	20.0359	8.5657
25	45.6945	51.3579	12.3941	42.8583	46.5296	8.5661	20.2163	22.7282	12.4251	19.137	20.7763	8.5661
50	45.9764	51.6761	12.3970	43.2277	46.9306	8.5660	20.8528	23.4463	12.4372	19.9566	21.6661	8.5661
100	46.5351	52.3067	12.4027	43.9571	47.7225	8.5661	22.0708	24.8204	12.4581	21.5024	23.3443	8.5660
							λ_3					
0	78.0220	87.6756	12.3729	73.1538	79.4202	8.5661	45.4547	51.087	12.3910	42.5265	46.1694	8.5662
5	78.0546	87.7123	12.3730	73.1967	79.4668	8.5661	45.5115	51.1511	12.3916	42.6012	46.2505	8.5662
25	78.1845	87.8591	12.3741	73.3681	79.6529	8.5661	45.7381	51.4069	12.3940	42.8987	46.5735	8.5662
50	78.3467	88.0421	12.3750	73.5819	79.8850	8.5661	46.0198	51.7248	12.3968	43.2678	46.9741	8.5660
100	78.6700	88.4071	12.3771	74.0075	80.3471	8.5662	46.578	52.3549	12.4026	43.9966	47.7654	8.5661

Neglecting the effect of the elastic foundation parameter, K_w, the shear component of the elastic foundation parameter, K_p, has a significant effect on the vibration behavior of piezoelectric composite beams. The dependency of the resonant frequency parameters of the first lowest three vibration modes on the nondimensional foundation parameter, K_p, at different values of the material Poisson's ratio for nonclassical and classical electromechanical and mechanical behaviors are illustrated in Figure 4. It is observed that the nondimensional fundamental frequency parameter is nonlinearly dependent on the nondimensional elastic foundation parameter, K_p. Increasing the nondimensional elastic foundation parameter, K_p, results in increasing the nondimensional frequency parameter. Contrary to the detected trend for the effect of K_w, increasing the nondimensional foundation parameter, K_p, is significant for higher vibration modes.

Table 6 illustrates the influence of the material Poisson's ratio on the nondimensional frequency parameters of the first lowest three vibration modes for electromechanical and mechanical nonclassical behaviors for CS and SS BCs at different values of the nondimensional elastic foundation parameter, K_p/π^2. It is observed that although the rate of increasing the nondimensional elastic foundation parameter K_p is smaller than that of K_w, it produces a relative percentage difference of about 12.5% for the nonclassical electromechanical behavior and about 8.6% for the nonclassical mechanical behavior for both CS and SS beam BCs.

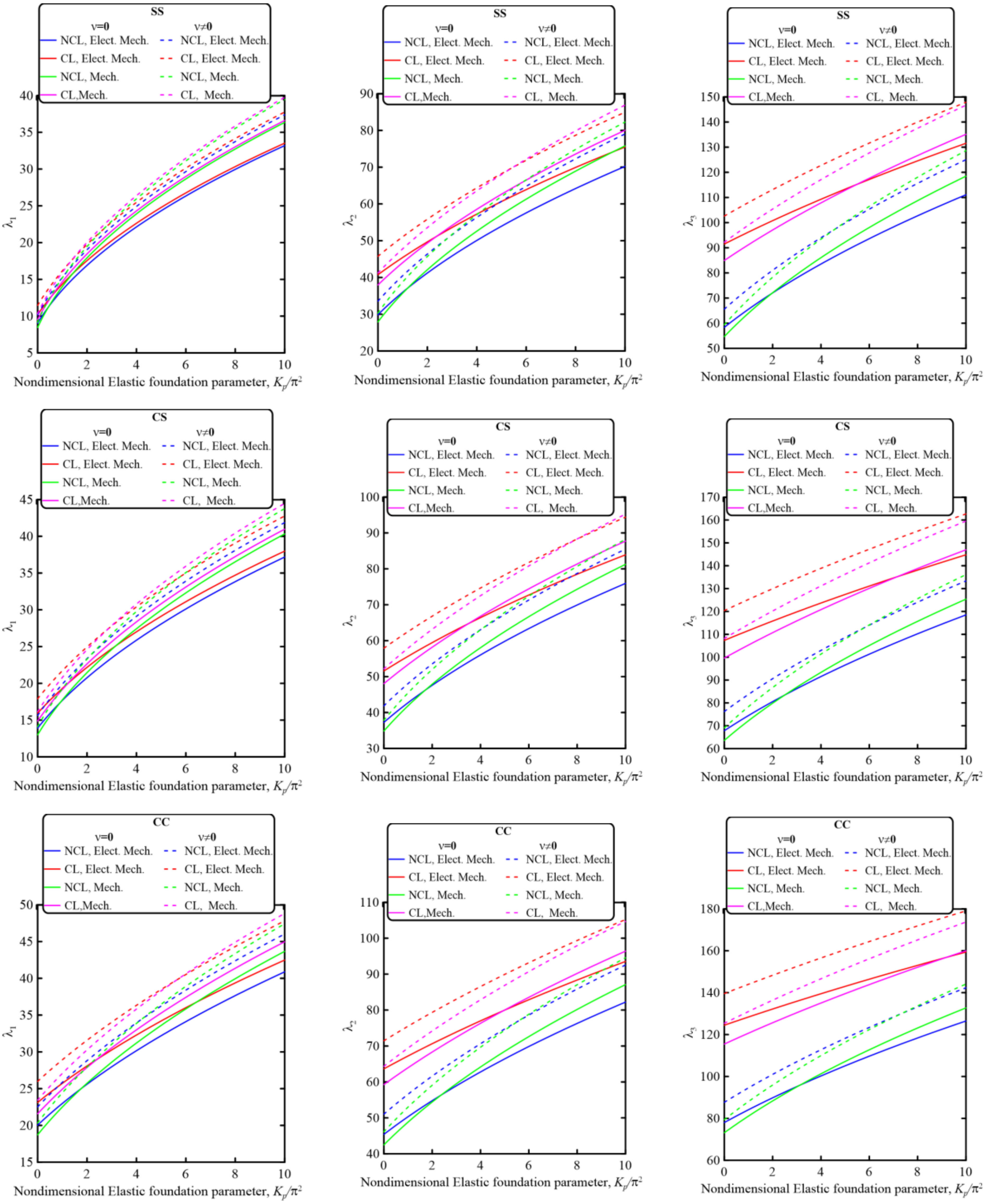

Figure 4. *Cont.*

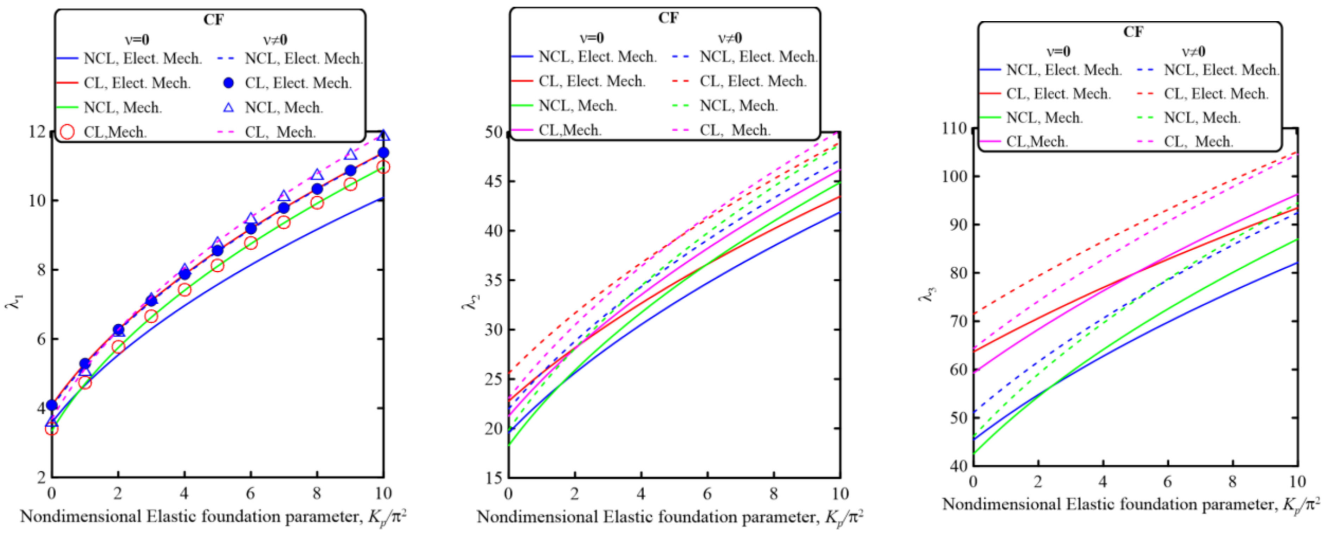

Figure 4. Dependency of the resonant frequency parameters for the lowest three vibration modes on the nondimensional foundation parameter, K_p, at different values of Poisson's ratio, ν for nonclassical and classical behaviors of piezoelectric composite nanobeams for different beam BCs, at N = 4 and beam aspect ratio, L/h = 20, N = 4, e_0a/h = 4, l/h = 2, K_w = 0., ν_c = 0.24, and ν_p = 0.27.

Table 6. Effect of the material Poisson's ratio on the frequency parameters of the first three vibration modes for electromechanical and mechanical nonclassical behaviors for CS and SS BCs at different values of the nondimensional elastic foundation parameter, K_p/π^2 for N = 4 and beam aspect ratio, L/h = 20, e_0a/h = 4, l/h = 2, α = 0.5, K_w = 0, ν_c = 0.24, and ν_p = 0.27.

	CS						SS					
K_p/π^2	NCL_Elect		%E	NCL_Mech		%E	NCL_Elect		%E	NCL_Mech		%E
	ν = 0	ν ≠ 0		ν = 0	ν ≠ 0		ν = 0	ν ≠ 0		ν = 0	ν ≠ 0	
							λ_1					
0	13.9087	15.6351	12.4124	12.999	14.1125	8.5660	9.0454	10.1683	12.4140	8.4535	9.1776	8.5657
0.5	15.9026	17.8847	12.4640	15.5506	16.8827	8.5662	11.5242	12.9644	12.4972	11.5731	12.5644	8.5656
2.5	22.1508	24.9297	12.5454	23.0914	25.0695	8.5664	18.3509	20.6592	12.5787	19.5917	21.27	8.5664
5	28.069	31.5995	12.5779	29.9575	32.5237	8.5661	24.3247	27.39	12.6016	26.3858	28.646	8.5660
10	37.1791	41.8641	12.6012	40.3229	43.777	8.5661	33.1898	37.3769	12.6156	36.345	39.4584	8.5662
							λ_2					
0	37.2447	41.8602	12.3924	34.8416	37.8262	8.5662	29.8496	33.5493	12.3945	27.9204	30.3121	8.5661
0.5	40.0778	45.0576	12.4253	38.5146	41.8138	8.5661	33.0584	37.1703	12.4383	32.0581	34.8042	8.5660
2.5	49.8247	56.0519	12.4982	50.6075	54.9426	8.5661	43.5923	49.0502	12.5203	44.949	48.7994	8.5662
5	59.815	67.3153	12.5392	62.5164	67.8716	8.5661	53.9404	60.7149	12.5592	57.1076	61.9995	8.5661
10	75.9507	85.501	12.5743	81.2568	88.2173	8.5661	70.2007	79.0382	12.5889	75.7826	82.2743	8.5662
							λ_3					
0	67.8433	76.2383	12.3741	63.5966	69.0443	8.5660	58.3649	65.5879	12.3756	54.6992	59.3848	8.5661
0.5	71.2365	80.0685	12.3981	68.0314	73.859	8.5660	62.0726	69.7729	12.4053	59.5318	64.6314	8.5662
2.5	83.4407	93.8387	12.4615	83.4461	90.5942	8.5661	75.0946	84.4642	12.4771	75.843	82.3398	8.5661
5	96.5505	108.6238	12.5046	99.4081	107.9235	8.5661	88.7239	99.833	12.5210	92.2623	100.1655	8.5660
10	118.4959	133.3641	12.5474	125.3771	136.1171	8.5662	111.0738	125.0259	12.5611	118.4595	128.6068	8.5661

5.2.2. Effect of the Perforation Filling Ratio, α

Keeping the constant value of the number of holes throughout the perforated core cross-section, a comparison of the dependency of the resonant frequency parameters of the first lowest three vibration modes on the perforation filling ratio at different values of the material Poisson's ratio for different beam configurations for electromechanical and mechanical nonclassical and classical behaviors is depicted in Figure 5. It is seen that the nondimensional electromechanical and mechanical frequency parameters are nonlinearly decreased with increasing the perforation filling ratio due to the reduction in the stiffness to mass ratio of the perforated core for all beam configurations for nonclassical and classical behaviors. As indicated before, underestimated nondimensional frequency parameters are detected when the material Poisson's effect is neglected compared with the corresponding cases obtained by considering the material Poisson's effect.

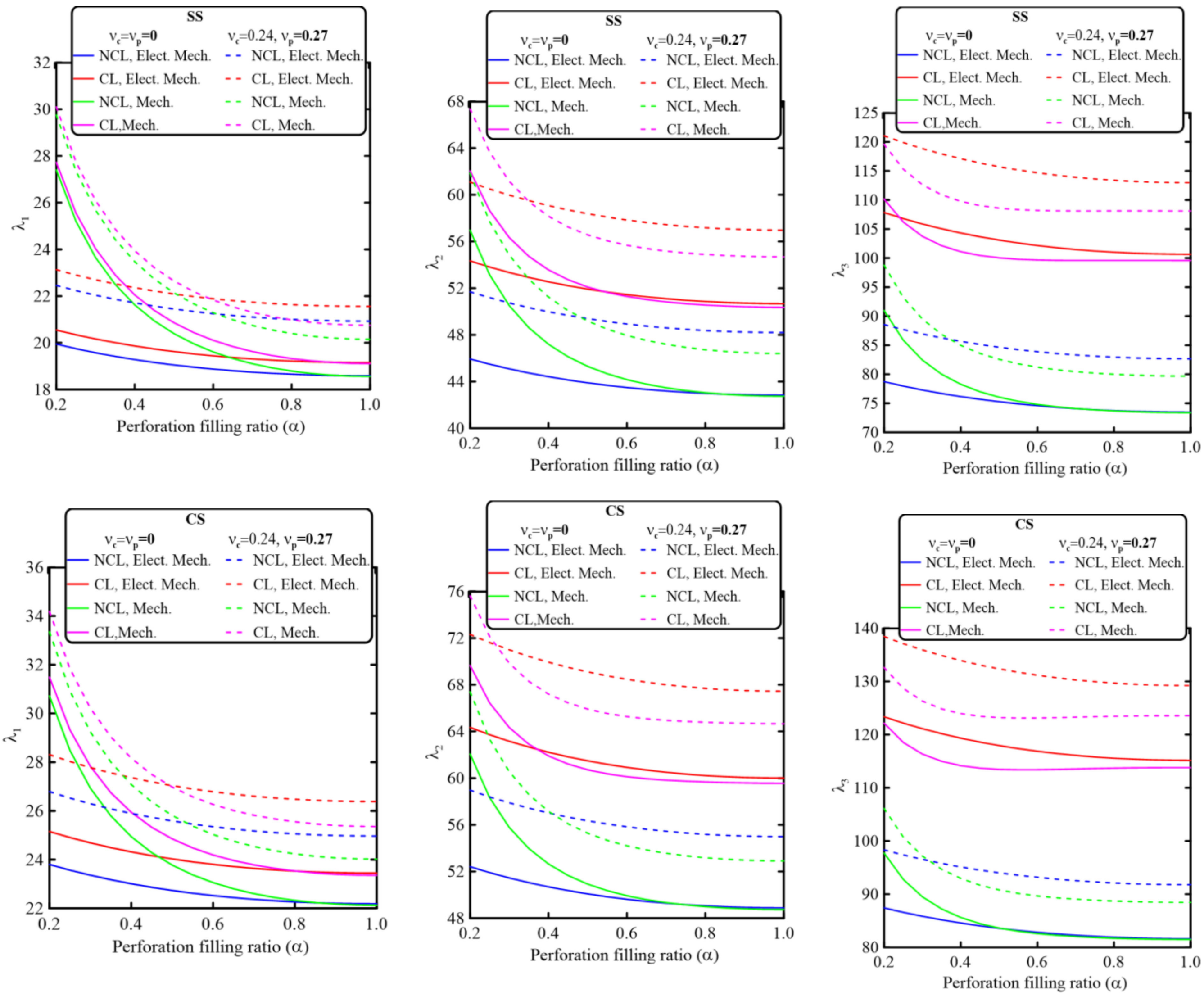

Figure 5. *Cont.*

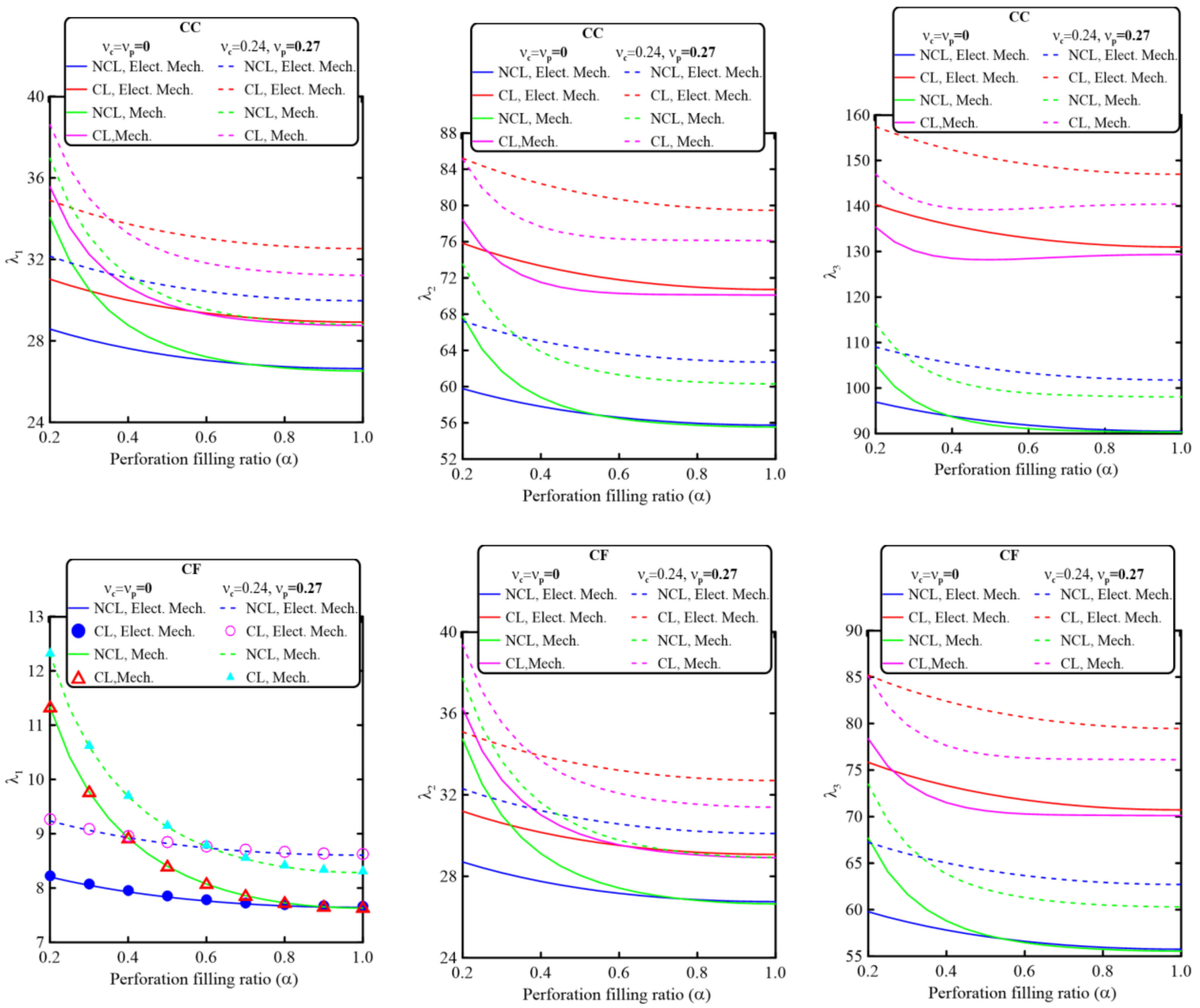

Figure 5. Comparison of the resonant frequency parameters of the lowest three vibration modes on the filling ratio, α at different values of Poisson's ratio for nonclassical and classical behaviors of piezoelectric composite nanobeams for different beam BCs, at N = 4 and beam aspect ratio, L/h = 20, e_0a/h = 4, l/h = 2, K_p/π^2 = 2.5, and K_w = 25.

5.2.3. Effect of the Number of Hole Rows, *N*

With a constant value of the perforation filling ratio, the dependency of the nondimensional frequency parameter on the number of hole rows, N, for electromechanical and mechanical nonclassical and classical behaviors for different BCs is depicted in Figure 6. It is observed that the nondimensional electromechanical frequency parameters are slightly increased with increasing the number of hole rows for all beam configurations, while different trends are observed for the mechanical behaviors depending on the beam configuration. It is also noticed that, neglecting the nonlocality effect, the introduction of the strain gradient effect results in a stiffening effect leading to producing larger values of the nonclassical nondimensional frequency parameters compared with the corresponding classical cases. On the other hand, the introduction of the nonlocality parameter in the absence of the strain gradient parameter results in softening effect leading to smaller values of the nonclassical nondimensional frequency parameters compared with the corresponding classical behaviors.

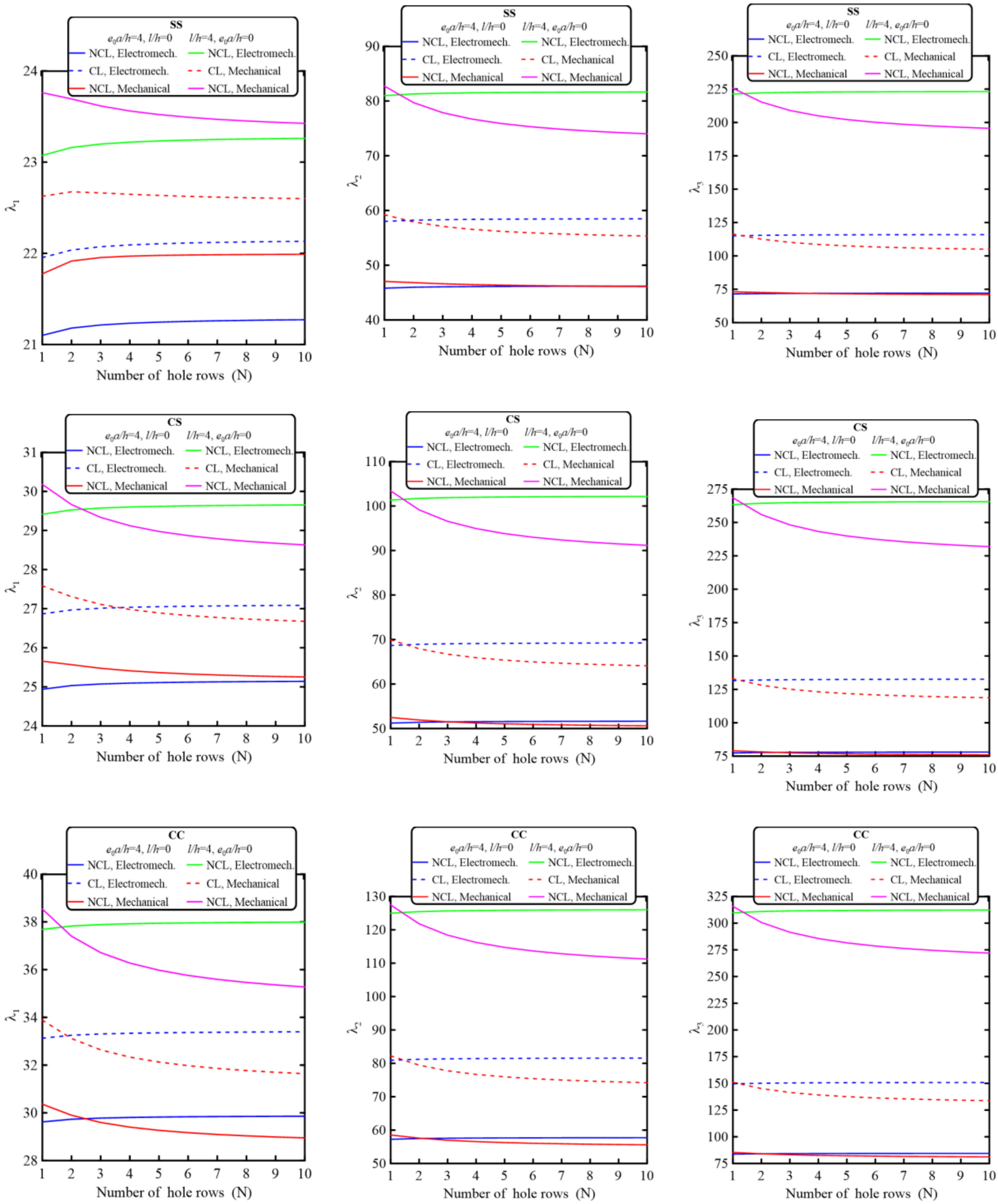

Figure 6. *Cont.*

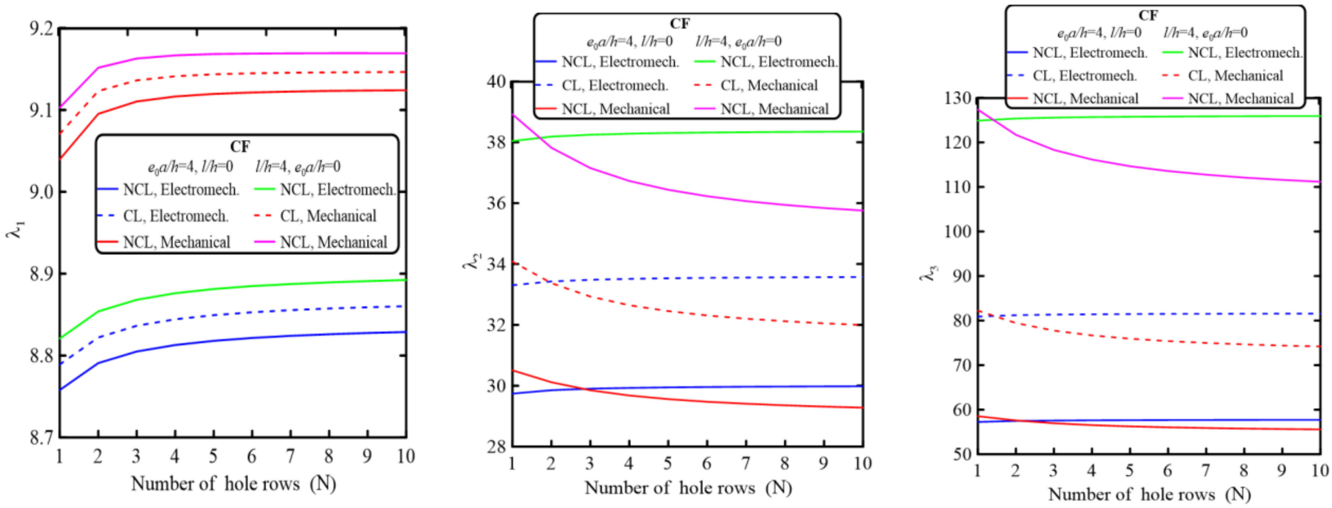

Figure 6. Dependency of the resonant frequency parameters on the number of holes, N for the first lowest three vibration modes at different values of Poisson's ratio for nonclassical and classical behaviors of piezoelectric composite nanobeams for different BCs, at $\alpha = 0.5$ and beam aspect ratio, $L/h = 20$, $K_p/\pi^2 = 2.5$, and $K_w = 25$.

5.2.4. Effect of the Nondimensional Strain Gradient Parameter, (l/h)

The dependency of the nondimensional frequency parameter on the dimensionless strain gradient parameter, *l/h*, for different beam configurations at different values of the material Poisson's ratio is demonstrated in Figure 7. It is observed that incorporating the strain gradient effect leads to increasing the overall system stiffness thus larger values of the resonant nondimensional frequency parameters are produced by increasing the strain gradient parameter for all vibration modes and BCs. Additionally, at the considered elastic foundation. the nonlocal parameters and the piezoelectric and flexoelectric effects result in smaller values of the electromechanical resonant frequency parameters compared with the corresponding mechanical behaviors. Furthermore, the material Poisson's effect produces larger values of the nondimensional resonant frequency parameters.

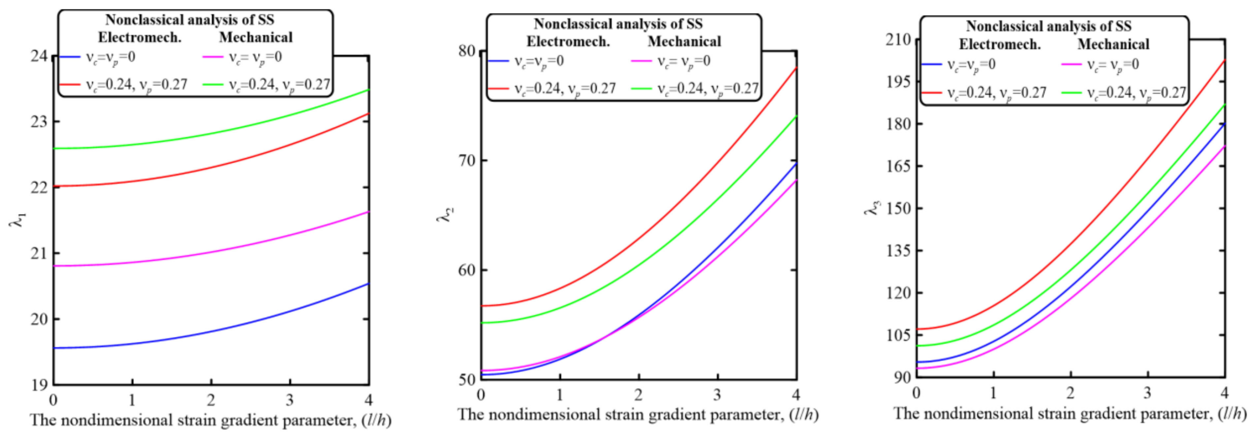

Figure 7. *Cont.*

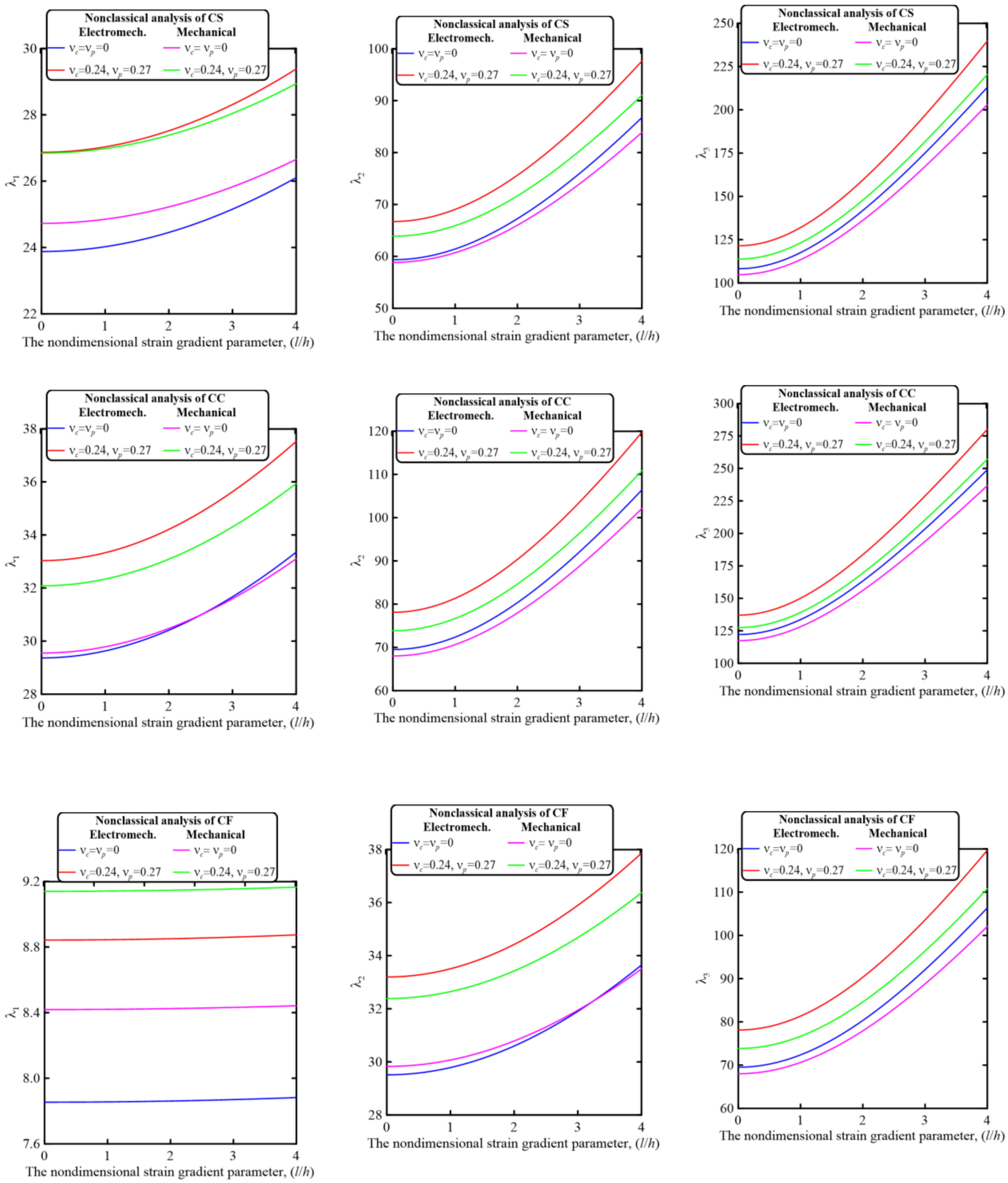

Figure 7. Dependency of the resonant frequency parameters on the nondimensional strain gradient parameter, l/h, for the lowest three vibration modes at different values of Poisson's ratio for nonclassical behaviors of piezoelectric composite nanobeams for different BCs at α = 0.5, N = 4, e_0a/h = 1, beam aspect ratio, L/h = 20, K_p/π^2 = 2.5, and K_w = 25.

5.2.5. Effect of the Nondimensional Nonlocal Parameter, (ea/h)

On the other hand, introducing the nonlocal effect results in a softening effect leading to produce smaller values of the resonant frequency parameters, as demonstrated in Figure 8. It is demonstrated that the nondimensional frequency parameters are nonlinearly decreased with increasing the nonlocal parameter due to the material softening effect. Smaller values of the nondimensional frequency parameters are detected due to ignoring the material Poisson's effect. Moreover, the introduction of the piezoelectric and flexoelectric effects produce smaller values of the resonant frequency parameter compared with the corresponding mechanical behavior at the first vibration mode. This effect may be reversed at higher vibration modes depending on the beam boundary condition.

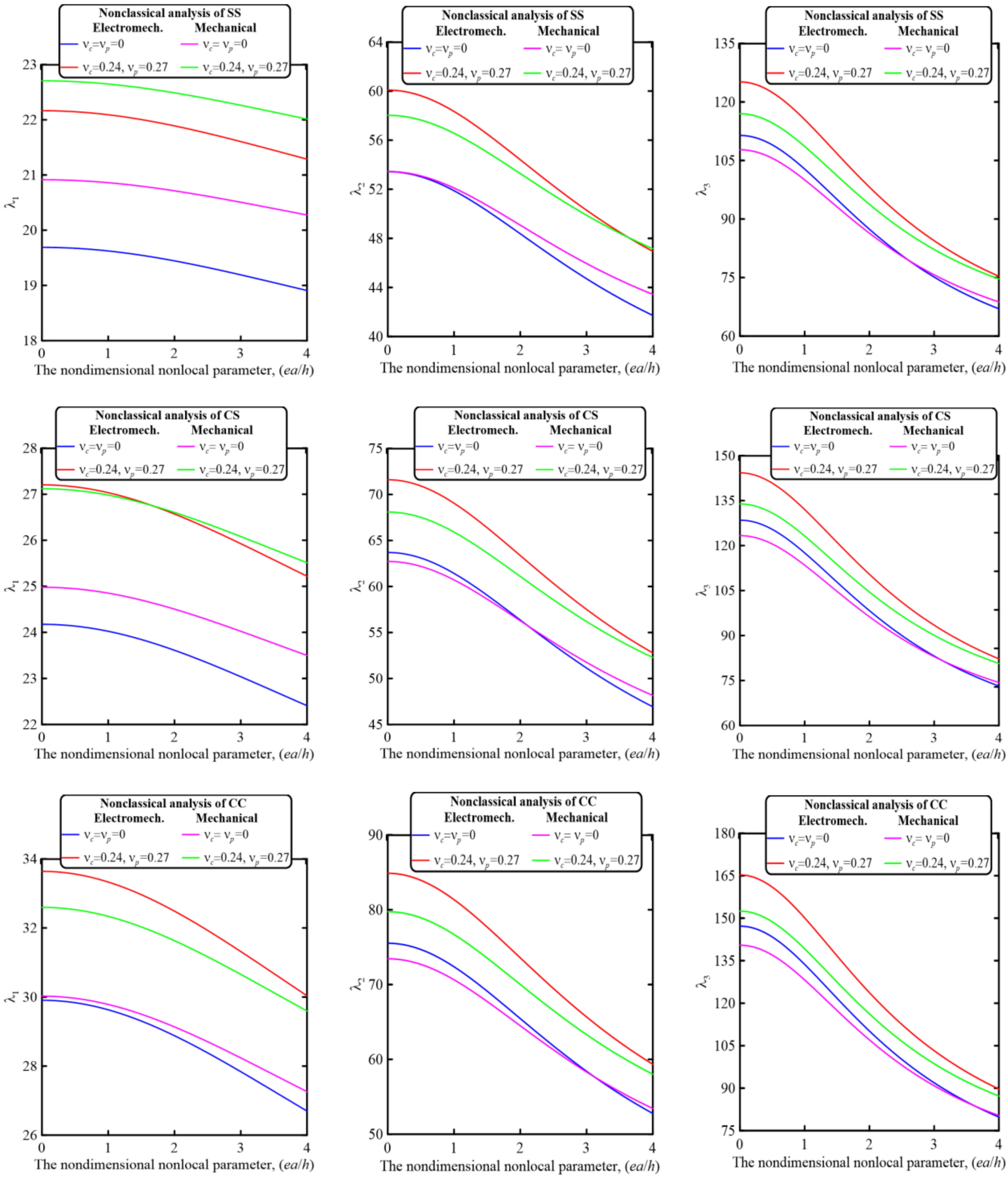

Figure 8. *Cont.*

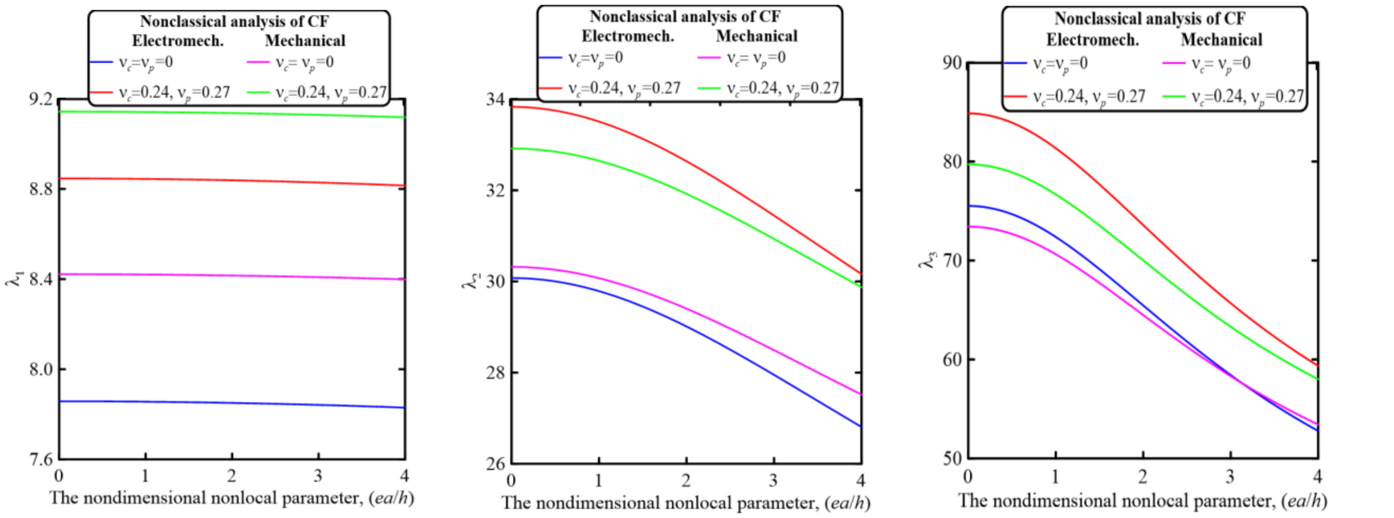

Figure 8. Dependency of the resonant frequency parameters on the nondimensional nonlocal parameter, ea/h, for the lowest three vibration modes at different values of Poisson's ratio for nonclassical behaviors of piezoelectric composite nanobeams for different BCs at α = 0.5, N = 4, e_0a/h = 1, beam aspect ratio, L/h = 20, K_p/π^2 = 2.5, and K_w = 25.

5.2.6. Effect of the Piezoelectric Coefficient, (e_{311})

The dependency of the electromechanical nondimensional frequency parameters on the piezoelectric coefficient, e_{311}, for the first lowest three vibration modes for nonclassical and classical behaviors for different beam configurations at different values of the material Poisson's ratio is demonstrated in Table 7. It may be noticed that increasing the absolute values of the piezoelectric coefficient, e_{311}, produces larger values of the nondimensional frequency parameters for all beam BCs. This effect becomes more significant at higher vibration modes.

5.2.7. Effect of Electric Field Strain Gradient Coupling Coefficient, (μ_{3111})

The electric field strain gradient coupling coefficient, μ_{3111}, significantly affects the electromechanical vibration behavior of the composite piezoelectric nanobeam. The dependency of the electromechanical nondimensional frequency parameters on the electric field strain gradient coupling coefficient, μ_{3111}, for the first lowest three vibration modes for different beam configurations at different values of the material Poisson's ratio is depicted in Table 8. It may be observed that increasing the absolute values of the electric field-strain gradient coupling coefficient results in a slight increase in the nondimensional fundamental resonant frequency parameter for all considered BCs. Moreover, the electromechanical behavior is significantly affected by considering the material Poisson's effect.

Table 7. Dependency of the resonant frequency parameters of the lowest three vibration modes with e_{311} for electromechanical behavior of piezoelectric composite nanobeams at different values of the elastic foundation parameters for different BCs at α = 0.5, N = 4, beam aspect ratio, L/h = 20, N = 4, e_0a/h = 1, l/h = 4, K_w = 25, K_p/π^2 = 2.5.

	SS				CC				CF				CS			
	NCL		CL		NCL		CL		NCL		CL		NCL		CL	
	$\nu_c = \nu_p = 0$	$\nu_c = 0.24$ $\nu_p = 0.27$	$\nu_c = \nu_p = 0$	$\nu_c = 0.24$ $\nu_p = 0.27$	$\nu_c = \nu_p = 0$	$\nu_c = 0.24$ $\nu_p = 0.27$	$\nu_c = \nu_p = 0$	$\nu_c = 0.24$ $\nu_p = 0.27$	$\nu_c = \nu_p = 0$	$\nu_c = 0.24$ $\nu_p = 0.27$	$\nu_c = \nu_p = 0$	$\nu_c = 0.24$ $\nu_p = 0.27$	$\nu_c = \nu_p = 0$	$\nu_c = 0.24$ $\nu_p = 0.27$	$\nu_c = \nu_p = 0$	$\nu_c = 0.24$ $\nu_p = 0.27$
e_{311}	λ_1															
−12	20.8663	23.4133	19.9738	22.4019	34.3647	38.4291	30.8067	34.3799	7.9924	8.9723	7.9665	8.943	26.7242	29.9311	24.7164	27.6506
−8	20.6624	23.2319	19.7555	22.2075	33.7303	37.8628	30.0753	33.726	7.9232	8.9107	7.8969	8.8811	26.3367	29.5856	24.2847	27.2654
−4	20.5392	23.1223	19.6234	22.09	33.3438	37.519	29.6278	33.3276	7.8813	8.8735	7.8549	8.8437	26.1014	29.3764	24.022	27.0317
0	20.4979	23.0857	19.5791	22.0507	33.214	37.4037	29.4771	33.1937	7.8673	8.8611	7.8408	8.8312	26.0225	29.3063	23.9338	26.9533
4	20.5392	23.1223	19.6234	22.09	33.3438	37.519	29.6278	33.3276	7.8813	8.8735	7.8549	8.8437	26.1014	29.3764	24.022	27.0317
8	20.6624	23.2319	19.7555	22.2075	33.7303	37.8628	30.0753	33.726	7.9232	8.9107	7.8969	8.8811	26.3367	29.5856	24.2847	27.2654
12	20.8663	23.4133	19.9738	22.4019	34.3647	38.4291	30.8067	34.3799	7.9924	8.9723	7.9665	8.943	26.7242	29.9311	24.7164	27.6506
	λ_2															
−12	71.1768	79.7641	53.9823	60.215	108.646	121.7285	76.0412	84.6213	34.6209	38.7283	30.9233	34.5215	88.5533	99.2212	64.2624	71.5872
−8	70.2932	78.9766	52.6948	59.0636	107.257	120.4904	73.8096	82.6218	34.012	38.185	30.2171	33.8904	87.4255	98.2161	62.5293	70.0356
−4	69.7576	78.5004	51.907	58.3618	106.415	119.7414	72.4376	81.3984	33.6414	37.8552	29.7853	33.506	86.7418	97.608	61.466	69.0879
0	69.5782	78.341	51.6417	58.126	106.132	119.4907	71.9744	80.9865	33.517	37.7447	29.64	33.3769	86.5127	97.4045	61.1075	68.7691
4	69.7576	78.5004	51.907	58.3618	106.415	119.7414	72.4376	81.3984	33.6414	37.8552	29.7853	33.506	86.7418	97.608	61.466	69.0879
8	70.2932	78.9766	52.6948	59.0636	107.257	120.4904	73.8096	82.6218	34.012	38.185	30.2171	33.8904	87.4255	98.2161	62.5293	70.0356
12	71.1768	79.7641	53.9823	60.215	108.646	121.7285	76.0412	84.6213	34.6209	38.7283	30.9233	34.5215	88.5533	99.2212	64.2624	71.5872
	λ_3															
−12	182.660	204.974	108.2391	120.337	252.201	283.0483	141.4364	157.043	108.590	121.6653	76.0419	84.6215	215.829	242.2106	124.1121	137.886
−8	181.122	203.605	105.0337	117.462	250.187	281.255	136.9017	152.971	107.199	120.425	73.8083	82.6201	214.059	240.6345	120.2659	134.435
−4	180.194	202.779	103.0627	115.703	248.970	280.1736	134.1074	150.476	106.355	119.6747	72.4351	81.3957	212.989	239.6839	117.898	132.321
0	179.883	202.503	102.3972	115.111	248.563	279.8121	133.1629	149.634	106.073	119.4236	71.9716	80.9835	212.632	239.3661	117.098	131.608
4	180.194	202.779	103.0627	115.703	248.970	280.1736	134.1074	150.476	106.355	119.6747	72.4351	81.3957	212.989	239.6839	117.898	132.321
8	181.122	203.605	105.0337	117.462	250.187	281.255	136.9017	152.971	107.199	120.425	73.8083	82.6201	214.059	240.6345	120.2659	134.435
12	182.660	204.974	108.2391	120.337	252.201	283.0483	141.4364	157.043	108.590	121.6653	76.0419	84.6215	215.829	242.2106	124.1121	137.886

Table 8. Dependency of the resonant frequency parameters of the lowest three vibration modes with μ_{3111} for electromechanical behavior of piezoelectric composite nanobeams at different values of the elastic foundation parameters for different BCs at α = 0.5, N = 4, beam aspect ratio, L/h = 20, N = 4, e_0a/h = 1, l/h = 4, K_w = 25, K_p/π^2 = 2.5.

$\mu_{3111} \times 10^8$	SS				CC				CF				CS			
	NCL		CL		NCL		CL		NCL		CL		NCL		CL	
	$\nu_c = \nu_p = 0$	$\nu_c = 0.24$ $\nu_p = 0.27$	$\nu_c = \nu_p = 0$	$\nu_c = 0.24$ $\nu_p = 0.27$	$\nu_c = \nu_p = 0$	$\nu_c = 0.24$ $\nu_p = 0.27$	$\nu_c = \nu_p = 0$	$\nu_c = 0.24$ $\nu_p = 0.27$	$\nu_c = \nu_p = 0$	$\nu_c = 0.24$ $\nu_p = 0.27$	$\nu_c = \nu_p = 0$	$\nu_c = 0.24$ $\nu_p = 0.27$	$\nu_c = \nu_p = 0$	$\nu_c = 0.24$ $\nu_p = 0.27$	$\nu_c = \nu_p = 0$	$\nu_c = 0.24$ $\nu_p = 0.27$
								λ_1								
−5	20.5413	23.1242	19.6256	22.092	33.3504	37.5248	29.6354	33.3344	7.882	8.8741	7.8556	8.8443	26.1054	29.3799	24.0265	27.0356
−2.5	20.5365	23.1199	19.6205	22.0874	33.3317	37.5082	29.6137	33.3151	7.8819	8.874	7.8554	8.8442	26.0948	29.3705	24.0146	27.0251
−1.25	20.5353	23.1189	19.6192	22.0863	33.327	37.5041	29.6083	33.3103	7.8819	8.874	7.8554	8.8442	26.0921	29.3681	24.0116	27.0224
0	20.5349	23.1185	19.6188	22.0859	33.3255	37.5027	29.6065	33.3087	7.8819	8.874	7.8554	8.8442	26.0912	29.3673	24.0106	27.0215
1.25	20.5353	23.1189	19.6192	22.0863	33.327	37.5041	29.6083	33.3103	7.8819	8.874	7.8554	8.8442	26.0921	29.3681	24.0116	27.0224
2.5	20.5365	23.1199	19.6205	22.0874	33.3317	37.5082	29.6137	33.3151	7.8819	8.874	7.8554	8.8442	26.0948	29.3705	24.0146	27.0251
5	20.5413	23.1242	19.6256	22.092	33.3504	37.5248	29.6354	33.3344	7.882	8.8741	7.8556	8.8443	26.1054	29.3799	24.0265	27.0356
								λ_2								
−5	69.7667	78.5084	51.9204	58.3737	106.429	119.754	72.461	81.4192	33.6477	37.8608	29.7926	33.5125	86.7534	97.6183	61.4841	69.104
−2.5	69.6838	78.4347	51.7979	58.2648	106.277	119.619	72.2115	81.1973	33.6284	37.8436	29.7701	33.4925	86.6384	97.516	61.3042	68.944
−1.25	69.663	78.4163	51.7672	58.2375	106.239	119.585	72.149	81.1417	33.6235	37.8393	29.7644	33.4874	86.6096	97.4905	61.2592	68.9039
0	69.6561	78.4101	51.757	58.2284	106.226	119.574	72.1281	81.1231	33.6219	37.8379	29.7625	33.4858	86.6	97.4819	61.2441	68.8906
1.25	69.663	78.4163	51.7672	58.2375	106.239	119.585	72.149	81.1417	33.6235	37.8393	29.7644	33.4874	86.6096	97.4905	61.2592	68.9039
2.5	69.6838	78.4347	51.7979	58.2648	106.277	119.619	72.2115	81.1973	33.6284	37.8436	29.7701	33.4925	86.6384	97.516	61.3042	68.944
5	69.7667	78.5084	51.9204	58.3737	106.429	119.754	72.461	81.4192	33.6477	37.8608	29.7926	33.5125	86.7534	97.6183	61.4841	69.104
								λ_3								
−5	180.209	202.793	103.096	115.733	248.991	280.192	134.155	150.518	106.370	119.687	72.4585	81.4165	213.007	239.70	117.938	132.357
−2.5	179.886	202.506	102.4037	115.117	248.519	279.773	133.06	149.543	106.218	119.552	72.2096	81.1951	212.613	239.350	117.057	131.572
−1.25	179.805	202.434	102.2298	114.962	248.401	279.668	132.785	149.298	106.180	119.519	72.1472	81.1396	212.515	239.262	116.835	131.375
0	179.778	202.410	102.1718	114.911	248.362	279.633	132.693	149.216	106.167	119.507	72.1264	81.1212	212.482	239.233	116.761	131.309
1.25	179.805	202.434	102.2298	114.962	248.401	279.668	132.785	149.298	106.180	119.519	72.1472	81.1396	212.515	239.262	116.835	131.375
2.5	179.886	202.506	102.4037	115.117	248.519	279.773	133.06	149.543	106.218	119.552	72.2096	81.1951	212.613	239.350	117.057	131.572
5	180.209	202.793	103.0962	115.733	248.991	280.192	134.155	150.518	106.370	119.687	72.4585	81.4165	213.007	239.70	117.938	132.357

6. Conclusions

Within the framework of the modified nonlocal strain gradient elasticity theory, a nonclassical analytical procedure is developed to investigate the electromechanical size-dependent free vibration behavior of piezoelectrically layered perforated nanobeam embedded in an elastic foundation considering flexoelectricity effects. The Poisson's effect is captured by applying the principles of three-dimensional continuum mechanics. All kinematics and kinetics relations are presented based on the EBBT. Regular squared perforation configuration is adopted for the perforated core. Hamilton's principle is utilized to develop the coupled electromechanical equation of motion. Closed forms for the resonant frequencies are derived for different BCs. The efficiency of the proposed procedure is verified by comparing the obtained results with the available results in the literature, and an excellent agreement is observed. Numerical experiments are depicted and discussed. The following concluding remarks are revealed:

- ➢ The elastic foundation significantly affects the electromechanical as well as the mechanical dynamic behavior of piezoelectrically layered perforated nanobeams embedded in an elastic media. The resonant frequencies and, consequently, the dynamic behavior could be controlled by controlling the elastic foundation parameters.
- ➢ The electromechanical resonant frequencies of piezoelectrically layered perforated nanobeams are increased with increasing the elastic foundation parameters due to increasing the overall system stiffness.
- ➢ The electromechanical vibration behavior is more sensitive to increasing the elastic foundation parameter, K_p, compared with increasing K_w.
- ➢ The electromechanical and mechanical dynamic behaviors of piezoelectric composite nanobeams are significantly affected by the material Poisson's ratio. Ignoring the effect of the material Poisson's ratio leads to underestimates of the nondimensional frequency parameters.
- ➢ Perforation configuration and parameters have significant effects on the electromechanical and mechanical dynamic behavior of piezoelectrically layered perforated nanobeams. Both electromechanical and mechanical vibration behaviors could be controlled by controlling the geometrical parameters of the perforation configuration.
- ➢ The nonclassical material parameters significantly affect the electromechanical as well as mechanical vibration behavior of piezoelectrically layered perforated nanobeam embedded in an elastic media. Both softening and stiffening effects could be incorporated by applying the modified nonlocal strain gradient theory. Incorporation of the strain gradient effect produces a stiffening effect, while the introduction of the nonlocality effect results in a softening effect.
- ➢ The electromechanical vibration behavior could be controlled by controlling the piezoelectricity as well as flexoelectricity parameters.

Author Contributions: M.S.A. (project administration, funding acquisition, data curation, and resources); A.A.A. (software, validation, formal analysis, investigation, and original draft); A.H. (formal analysis, investigation, resources, and original draft); H.M.A. (software, visualization, data curation, and formal analysis); M.A.E. (Conceptualization, methodology, and review and editing). All authors have read and agreed to the published version of the manuscript.

Funding: This research was funded by the Institutional Fund Projects under grant no. IFPIP: 1120-135-1443.

Data Availability Statement: Not applicable.

Acknowledgments: This research was funded by the Institutional Fund Projects under grant no. IFPIP (1120-135-1443). The authors gratefully acknowledge technical and financial support provided by the Ministry of Education and King Abdulaziz University, DSR in Jeddah, Saudi Arabia.

Conflicts of Interest: The authors declare no conflict of interest.

References

1. Bagheri, R.; Tadi Beni, Y. On the size-dependent nonlinear dynamics of viscoelastic/flexoelectric nanobeams. *J. Vib. Control* **2021**, *27*, 2018–2033. [CrossRef]
2. Liang, X.; Hu, S.; Shen, S. Effects of surface and flexoelectricity on a piezoelectric nanobeam. *Smart Mater. Struct.* **2014**, *23*, 035020. [CrossRef]
3. Bhaskar, U.K.; Banerjee, N.; Abdollahi, A.; Wang, Z.; Schlom, D.G.; Rijnders, G.; Catalan, G. A flexoelectric microelectromechanical system on silicon. *Nat. Nanotechnol.* **2016**, *11*, 263–266. [CrossRef] [PubMed]
4. Baroudi, S.; Najar, F.; Jemai, A. Static and dynamic analytical coupled field analysis of piezoelectric flexoelectric nanobeams: A strain gradient theory approach. *Int. J. Solids Struct.* **2018**, *135*, 110–124. [CrossRef]
5. Chu, L.; Dui, G.; Ju, C. Flexoelectric effect on the bending and vibration responses of functionally graded piezoelectric nanobeams based on general modified strain gradient theory. *Compos. Struct.* **2018**, *186*, 39–49. [CrossRef]
6. Ebrahimi, F.; Karimiasl, M. Nonlocal and surface effects on the buckling behavior of flexoelectric sandwich nanobeams. *Mech. Adv. Mater. Struct.* **2018**, *25*, 943–952. [CrossRef]
7. Wang, K.F.; Wang, B.L.; Zeng, S. Analysis of an array of flexoelectric layered nanobeams for vibration energy harvesting. *Compos. Struct.* **2018**, *187*, 48–57. [CrossRef]
8. Shijie, Z.; Xie, Z.; Wang, H. Theoretical and finite element modeling of piezoelectric nanobeams with surface and flexoelectricity effects. *Mech. Adv. Mater. Struct.* **2019**, *26*, 1261–1270. [CrossRef]
9. Basutkar, R. Analytical modelling of a nanoscale series-connected bimorph piezoelectric energy harvester incorporating the flexoelectric effect. *Int. J. Eng. Sci.* **2019**, *139*, 42–61. [CrossRef]
10. Eltaher, M.A.; Omar, F.A.; Abdalla, W.S.; Kabeel, A.M.; Alshorbagy, A.E. Mechanical analysis of cutout piezoelectric nonlocal nanobeam including surface energy effects. *Struct. Eng. Mech.* **2020**, *76*, 141–151. [CrossRef]
11. Eltaher, M.A.; Omar, F.A.; Abdraboh, A.M.; Abdalla, W.S.; Alshorbagy, A.E. Mechanical behaviors of piezoelectric nonlocal nanobeam with cutouts. *Smart Struct. Syst.* **2020**, *25*, 219–228. [CrossRef]
12. Zhao, X.; Zheng, S.; Li, Z. Effects of porosity and flexoelectricity on static bending and free vibration of AFG piezoelectric nanobeams. *Thin-Walled Struct.* **2020**, *151*, 106754. [CrossRef]
13. Malikan, M.; Eremeyev, V.A. On the dynamics of a visco–piezo–flexoelectric nanobeam. *Symmetry* **2020**, *12*, 643. [CrossRef]
14. Malikan, M.; Eremeyev, V.A. On nonlinear bending study of a piezo-flexomagnetic nanobeam based on an analytical-numerical solution. *Nanomaterials* **2020**, *10*, 1762. [CrossRef]
15. Malikan, M. Electro-mechanical shear buckling of piezoelectric nanoplate using modified couple stress theory based on simplified first order shear deformation theory. *Appl. Math. Model.* **2017**, *48*, 196–207. [CrossRef]
16. Malikan, M.; Eremeyev, V.A. Flexomagnetic response of buckled piezomagnetic composite nanoplates. *Compos. Struct.* **2021**, *267*, 113932. [CrossRef]
17. Esen, I.; Abdelrhmaan, A.A.; Eltaher, M.A. Free vibration and buckling stability of FG nanobeams exposed to magnetic and thermal fields. *Eng. Comput.* **2022**, *38*, 3463–3482. [CrossRef]
18. Esen, I.; Özarpa, C.; Eltaher, M.A. Free vibration of a cracked FG microbeam embedded in an elastic matrix and exposed to magnetic field in a thermal environment. *Compos. Struct.* **2021**, *261*, 113552. [CrossRef]
19. Wang, Y.Q.; Liu, Y.F.; Yang, T.H. Nonlinear thermo-electro-mechanical vibration of functionally graded piezoelectric nanoshells on Winkler–Pasternak foundations via nonlocal Donnell's nonlinear shell theory. *Int. J. Struct. Stab. Dyn.* **2019**, *19*, 1950100. [CrossRef]
20. Liu, Y.; Qin, Z.; Chu, F. Nonlinear forced vibrations of functionally graded piezoelectric cylindrical shells under electric-thermo-mechanical loads. *Int. J. Mech. Sci.* **2021**, *201*, 106474. [CrossRef]
21. Liu, Y.; Qin, Z.; Chu, F. Nonlinear forced vibrations of FGM sandwich cylindrical shells with porosities on an elastic substrate. *Nonlinear Dyn.* **2021**, *104*, 1007–1021. [CrossRef]
22. Gao, W.; Liu, Y.; Qin, Z.; Chu, F. Wave propagation in smart sandwich plates with functionally graded nanocomposite porous core and piezoelectric layers in multi-physics environment. *Int. J. Appl. Mech.* **2022**, *14*, 2250071. [CrossRef]
23. Melaibari, A.; Abdelrahman, A.A.; Hamed, M.A.; Abdalla, A.W.; Eltaher, M.A. Dynamic Analysis of a Piezoelectrically Layered Perforated Nonlocal Strain Gradient Nanobeam with Flexoelectricity. *Mathematics* **2022**, *10*, 2614. [CrossRef]
24. Jena, S.K.; Chakraverty, S.; Mahesh, V.; Harursampath, D.; Sedighi, H.M. A novel numerical approach for the stability of nanobeam exposed to hygro-thermo-magnetic environment embedded in elastic foundation. *ZAMM-J. Appl. Math. Mech.* **2022**, *102*, e202100380. [CrossRef]
25. Sun, R.; Liu, D.; Yan, Z. A finite element approach for flexoelectric nonuniform nanobeam energy harvesters. *Mech. Adv. Mater. Struct.* **2022**, 1–12. [CrossRef]
26. Thai, T.Q.; Zhuang, X.; Rabczuk, T. Curved flexoelectric and piezoelectric micro-beams for nonlinear vibration analysis of energy harvesting. *Int. J. Solids Struct.* **2023**, *264*, 112096. [CrossRef]
27. Momeni-Khabisi, H.; Tahani, M. Coupled thermal stability analysis of piezomagnetic nano-sensors and nano-actuators considering the flexomagnetic effect. *Eur. J. Mech. A/Solids* **2023**, *97*, 104773. [CrossRef]
28. Jena, S.K.; Chakraverty, S.; Tornabene, F. Dynamical behavior of nanobeam embedded in constant, linear, parabolic, and sinusoidal types of Winkler elastic foundation using first-order nonlocal strain gradient model. *Mater. Res. Express* **2019**, *6*, 0850f2. [CrossRef]

29. Jena, S.K.; Chakraverty, S. Dynamic analysis of single-layered graphene nano-ribbons (SLGNRs) with variable cross-section resting on elastic foundation. *Curved Layer. Struct.* **2019**, *6*, 132–145. [CrossRef]
30. Jena, S.K.; Chakraverty, S.; Malikan, M.; Mohammad-Sedighi, H. Hygro-magnetic vibration of the single-walled carbon nanotube with nonlinear temperature distribution based on a modified beam theory and nonlocal strain gradient model. *Int. J. Appl. Mech.* **2020**, *12*, 2050054. [CrossRef]
31. Malikan, M.; Krasheninnikov, M.; Eremeyev, V.A. Torsional stability capacity of a nano-composite shell based on a nonlocal strain gradient shell model under a three-dimensional magnetic field. *Int. J. Eng. Sci.* **2020**, *148*, 103210. [CrossRef]
32. Karami, B.; Janghorban, M.; Rabczuk, T. Dynamics of two-dimensional functionally graded tapered Timoshenko nanobeam in thermal environment using nonlocal strain gradient theory. *Compos. Part B Eng.* **2020**, *182*, 107622. [CrossRef]
33. Chakraverty, S.; Jena, S.K. Free vibration of single walled carbon nanotube resting on exponentially varying elastic foundation. *Curved Layer. Struct.* **2018**, *5*, 260–272. [CrossRef]
34. Abdelrahman, A.A.; Esen, I.; Daikh, A.A.; Eltaher, M.A. Dynamic analysis of FG nanobeam reinforced by carbon nanotubes and resting on elastic foundation under moving load. *Mech. Based Des. Struct. Mach.* **2021**, 1–24. [CrossRef]
35. Tocci Monaco, G.; Fantuzzi, N.; Fabbrocino, F.; Luciano, R. Trigonometric solution for the bending analysis of magneto-electro-elastic strain gradient nonlocal nanoplates in hygro-thermal environment. *Mathematics* **2021**, *9*, 567. [CrossRef]
36. Ghandourah, E.E.; Daikh, A.A.; Alhawsawi, A.M.; Fallatah, O.A.; Eltaher, M.A. Bending and Buckling of FG-GRNC Laminated Plates via Quasi-3D Nonlocal Strain Gradient Theory. *Mathematics* **2022**, *10*, 1321. [CrossRef]
37. Alazwari, M.A.; Esen, I.; Abdelrahman, A.A.; Abdraboh, A.M.; Eltaher, M.A. Dynamic analysis of functionally graded (FG) nonlocal strain gradient nanobeams under thermo-magnetic fields and moving load. *Adv. Nano Res.* **2022**, *12*, 231–251. [CrossRef]
38. Alam, M.; Mishra, S.K. A boundary layer solution for the post-critical thermo-electro-mechanical stability of nonlocal-strain gradient Functionally Graded Piezoelectric cylindrical shells. *Eur. J. Mech. A/Solids* **2023**, *97*, 104836. [CrossRef]
39. Boyina, K.; Piska, R. Wave propagation analysis in viscoelastic Timoshenko nanobeams under surface and magnetic field effects based on nonlocal strain gradient theory. *Appl. Math. Comput.* **2023**, *439*, 127580. [CrossRef]
40. Luschi, L.; Pieri, F. An analytical model for the determination of resonance frequencies of perforated beams. *J. Micromech. Microeng.* **2014**, *24*, 055004. [CrossRef]
41. Abdelrahman, A.A.; Eltaher, M.A. On bending and buckling responses of perforated nanobeams including surface energy for different beams theories. *Eng. Comput.* **2022**, *38*, 2385–2411. [CrossRef]
42. Zeng, S.; Wang, K.; Wang, B.; Wu, J. Vibration analysis of piezoelectric sandwich nanobeam with flexoelectricity based on nonlocal strain gradient theory. *Appl. Math. Mech.* **2020**, *41*, 859–880. [CrossRef]
43. Eftekhari, S.A.; Toghraie, D. Vibration and dynamic analysis of a cantilever sandwich microbeam integrated with piezoelectric layers based on strain gradient theory and surface effects. *Appl. Math. Comput.* **2022**, *419*, 126867. [CrossRef]
44. Abdelrahman, A.A.; Mohamed, N.A.; Eltaher, M.A. Static bending of perforated nanobeams including surface energy and microstructure effects. *Eng. Comput.* **2022**, *38*, 415–435. [CrossRef]
45. Mehralian, F.; Beni, Y.T. Vibration analysis of size-dependent bimorph functionally graded piezoelectric cylindrical shell based on nonlocal strain gradient theory. *J. Braz. Soc. Mech. Sci. Eng.* **2018**, *40*, 1–15. [CrossRef]
46. Abdelrahman, A.A.; Eltaher, M.A.; Kabeel, A.M.; Abdraboh, A.M.; Hendi, A.A. Free and forced analysis of perforated beams. *Steel Compos. Struct.* **2019**, *31*, 489–502. [CrossRef]
47. Eltaher, M.A.; Mohamed, N.; Mohamed, S.A.; Seddek, L.F. Periodic and nonperiodic modes of postbuckling and nonlinear vibration of beams attached to nonlinear foundations. *Appl. Math. Model.* **2019**, *75*, 414–445. [CrossRef]
48. Chanthanumataporn, S.; Watanabe, N. Free vibration of a light sandwich beam accounting for ambient air. *J. Vib. Control* **2018**, *24*, 3658–3675. [CrossRef]
49. Ke, L.L.; Wang, Y.S.; Wang, Z.D. Nonlinear vibration of the piezoelectric nanobeams based on the nonlocal theory. *Compos. Struct.* **2012**, *94*, 2038–2047. [CrossRef]
50. Chen, W.Q.; Lü, C.F.; Bian, Z.G. A mixed method for bending and free vibration of beams resting on a Pasternak elastic foundation. *Appl. Math. Model.* **2004**, *28*, 877–890. [CrossRef]
51. De Rosa, M.A.; Maurizi, M.J. The influence of concentrated masses and Pasternak soil on the free vibrations of Euler beams—Exact solution. *J. Sound Vib.* **1998**, *212*, 573–581. [CrossRef]